Deep–Sea Research I 189 (2022) 103854

Contents lists available at ScienceDirect

Deep-Sea Research Part I

journal homepage: www.elsevier.com/locate/dsri

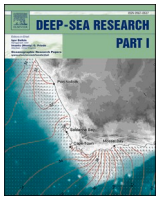

Hydrography and food distribution during a tidal cycle above a cold-water coral mound

Evert de Froe [a,*], Sandra R. Maier [b,c], Henriette G. Horn [b,d], George A. Wolff [e], Sabena Blackbird [e], Christian Mohn [f], Mads Schultz [g], Anna-Selma van der Kaaden [b], Chiu H. Cheng [b,i], Evi Wubben [h], Britt van Haastregt [b], Eva Friis Moller [f], Marc Lavaleye [a], Karline Soetaert [b], Gert-Jan Reichart [a,h], Dick van Oevelen [b]

[a] NIOZ Royal Netherlands Institute for Sea Research, Department of Ocean Systems, PO Box 59, 1790, AB, Den Burg, the Netherlands
[b] NIOZ Royal Netherlands Institute for Sea Research, Department of Estuarine and Delta Systems, PO Box 140, 4400, AC, Yerseke, the Netherlands
[c] Greenland Climate Research Centre, Greenland Institute of Natural Resources, Kivioq 2, PO Box 570, 3900, Nuuk, Greenland
[d] Centre for Coastal Research, University of Agder, PO Box 422, 4604, Kristiansand, Norway
[e] School of Environmental Sciences, University of Liverpool, 4 Brownlow Street, Liverpool, L69 3GP, UK
[f] Department of Ecoscience, Aarhus University, Frederiksborgvej 399, 4000, Roskilde, Denmark
[g] NORD University, Faculty of Biosciences and Aquaculture, Post Box 1490, 8049, Bodø, Norway
[h] Department of Earth Sciences, Faculty of Geosciences, Utrecht University, Princetonlaan 8a, 3584 CB Utrecht, the Netherlands
[i] Wageningen Marine Research, Wageningen University & Research, 4400 AB Yerseke, the Netherlands

ARTICLE INFO

Keywords:
Cold-water corals
Benthic-pelagic coupling
Organic matter transport
Internal waves
Diurnal tidal cycle
Particulate organic matter

ABSTRACT

Cold-water corals (CWCs) are important ecosystem engineers in the deep sea that provide habitat for numerous species and can form large coral mounds. These mounds influence surrounding currents and induce distinct hydrodynamic features, such as internal waves and episodic downwelling events that accelerate transport of organic matter towards the mounds, supplying the corals with food. To date, research on organic matter distribution at coral mounds has focussed either on seasonal timescales or has provided single point snapshots. Data on food distribution at the timescale of a diurnal tidal cycle is currently limited. Here, we integrate physical, biogeochemical, and biological data throughout the water column and along a transect on the south-eastern slope of Rockall Bank, Northeast Atlantic Ocean. This transect consisted of 24-h sampling stations at four locations: Bank, Upper slope, Lower slope, and the Oreo coral mound. We investigated how the organic matter distribution in the water column along the transect is affected by tidal activity. Repeated CTD casts indicated that the water column above Oreo mound was more dynamic than above other stations in multiple ways. First, the bottom water showed high variability in physical parameters and nutrient concentrations, possibly due to the interaction of the tide with the mound topography. Second, in the surface water a diurnal tidal wave replenished nutrients in the photic zone, supporting new primary production. Third, above the coral mound an internal wave (200 m amplitude) was recorded at 400 m depth after the turning of the barotropic tide. After this wave passed, high quality organic matter was recorded in bottom waters on the mound coinciding with shallow water physical characteristics such as high oxygen concentration and high temperature. Trophic markers in the benthic community suggest feeding on a variety of food sources, including phytodetritus and zooplankton. We suggest that there are three transport mechanisms that supply food to the CWC ecosystem. First, small phytodetritus particles are transported downwards to the seafloor by advection from internal waves, supplying high quality organic matter to the CWC reef community. Second, the shoaling of deeper nutrient-rich water into the surface water layer above the coral mound could stimulate diatom growth, which form fast-sinking aggregates. Third, evidence from lipid analysis indicates that zooplankton faecal pellets also enhance supply of organic matter to the reef communities. This study is the first to report organic matter quality and composition over a tidal cycle at a coral mound and provides evidence that fresh high-quality organic matter is transported towards a coral reef during a tidal cycle.

* Corresponding author.
E-mail addresses: evert.de.froe@nioz.nl, e.defroe@outlook.com (E. de Froe).

https://doi.org/10.1016/j.dsr.2022.103854
Received 4 April 2022; Received in revised form 14 August 2022; Accepted 16 August 2022
Available online 28 August 2022

1. Introduction

Framework-building cold-water corals (CWCs) are important ecosystem engineers in the deep sea and provide habitat for numerous species (Roberts et al., 2006). The CWC reefs can form large carbonate mounds ten to hundreds of metres high and several kilometres wide (Kenyon et al., 2003; van Weering et al., 2003). Carbonate mounds alter the surrounding hydrodynamic environment in various ways by enhancing current velocities (Mienis et al., 2007; Mohn et al., 2014), inducing episodic downward transport of waters from shallower depths (Davies et al., 2009; Soetaert et al., 2016), and breaking of internal waves (van Haren et al., 2014; Cyr et al., 2016). The interaction of the tide (barotropic) with the topography generates internal (baroclinic) tidal processes, which enhance mixing and transport of fresh organic matter, produced at the sunlit surface ocean, to the coral mounds (Duineveld et al., 2004, 2012). Benthic communities on the coral mounds require high-quality organic matter to survive in a food-limited deep-sea environment (Duineveld et al., 2007). Previous work has shown that suspended particulate organic matter (sPOM) in the vicinity of CWCs is of higher quality than at similar water depths in the open ocean (Kiriakoulakis et al., 2007). To date, little is known about the variability of organic matter quality during tidal cycles, and how tidal activity influences the organic matter distribution in the water column close to coral mounds (Duineveld et al., 2007).

The diverse CWC reef communities exhibit a suite of feeding strategies. Scleractinian corals, such as *Desmophyllum pertusum* (formerly *Lophelia pertusa*; Addamo et al., 2016) and *Madrepora oculata*, are opportunistic passive filter feeders that retain a variety of food sources such as fresh phytoplankton (Maier et al., 2019), sPOM, bacteria (Mueller et al., 2014), dissolved organic matter (DOM; Gori et al., 2014), and zooplankton (Carlier et al., 2009; Purser et al., 2010; Naumann et al., 2011; Larsson et al., 2013; Gori et al., 2015). Other passive suspension feeders (i.e. crinoids, stylasterids, ophiuroids, hydrozoans, bryozoans) live in-between or on the coral framework and also trap particles and DOM from the water column (Duineveld et al., 2007; Henry and Roberts, 2007; Maier et al., 2021). The active filter feeders, including sponges and bivalves, pump water to filter particles from the water (Van Soest and Lavaleye, 2005; Bart et al., 2020; Maier et al., 2020a). Polychaetes (i.e. *Eunice norvegica*) feed on larger particles caught by coral polyps but also have a predatory feeding mode (Mortensen, 2001; Roberts et al., 2009; Mueller et al., 2014; van Oevelen et al., 2018). The breadth and versatility of these feeding strategies suggest that CWC ecosystems can rely on a wide variety of organic matter sources.

A quantitative estimate of organic matter composition and quality in the water column could provide insight into the relative importance of each organic matter component (DOM, bacteria, sPOM, zooplankton) as a food source for the diverse reef community. Additionally, measurements on variability in organic matter composition over a full diurnal tidal cycle could resolve the effect of tidal forcing on organic matter availability and transport. Few studies have measured the *in-situ* distribution and composition of the whole organic matter spectrum above CWC reefs; sediment traps and long-term moorings have been used to show that food sources such as phytoplankton and zooplankton vary in abundance at CWC reefs on diurnal (Maier et al., 2019; Van Engeland et al., 2019) and seasonal timescales (Duineveld et al., 2004; Mienis et al., 2009a). Furthermore, the combination of physical transport and biotic degradation determine the rate at which sPOM is modified in the ocean interior and the quality of organic matter that reaches the seafloor. Quality of organic matter is an important proxy to determine sPOM palatability for the reef community, as on sinking from the mixed layer, remineralization processes by archaea/bacteria and consumption by zooplankton changes sPOM quality and hence palatability (Cho and Azam, 1988; Lampitt et al., 1993; Steinberg, 1995).

The south-eastern slope of Rockall Bank (Fig. 1 A and B) is an area with numerous coral carbonate mounds hosting thriving CWC reefs (Kenyon et al., 2003). Previous work has described large amplitude (100–200 m) diurnal tidal waves (Mienis et al., 2007; van Haren et al., 2014) and biodiverse benthic communities living in this reefs, which feed primarily on phytodetritus (Duineveld et al., 2007; van Oevelen et al., 2009). Moreover, long-term seasonal studies revealed the arrival of a spring bloom on the seafloor in March/April, and more degraded organic matter in winter (Duineveld et al., 2007; Mohn and White, 2007; Mienis et al., 2009a). A modelling study suggests that there is a large mismatch between the high amount of organic matter required to sustain CWC reef metabolism and the comparatively low organic matter flux to the reef measured by sediment traps (van Oevelen et al., 2009). However, the organic matter transport pathways towards CWC reefs are still in debate. Some studies suggest cross-slope transport of organic matter from a shallower part of the Rockall Bank towards the coral mounds by the presence of intermediate nepheloid layers (Mienis et al., 2007; Bourgault et al., 2014), and 'Ekman drainage' (White et al., 2005; Simpson and McCandliss, 2013). Furthermore, a modelling study indicates the possibility of vertical transport of fresh organic matter during spring tide conditions (Soetaert et al., 2016).

This study set out to investigate the organic matter distribution along the south-eastern (SE) slope of Rockall Bank and to determine the effect of tidal dynamics on organic matter distribution in the water column. By measuring the hydrography and organic matter composition throughout the water column during a full 24-h tidal cycle along a transect from the shallow (±450 m) bank to a deep (±800 m) carbonate mound CWC reef, we aim to (i) assess the organic matter distribution in the water column along the transect and (ii) investigate how the tidal activity affects this organic matter distribution. Additionally, (iii) we attempt to unravel the importance of each potential food source (sPOM, bacteria, zooplankton) for the seafloor communities.

2. Material and methods

2.1. Study area

The study area is located on the SE Rockall Bank slope, 500 km west of Ireland (Fig. 1A and B). Rockall Bank is a large submarine bank, with the seafloor mostly composed of soft sediment on the top and coral ridges and mounds are found on the SE slope between 400 and 1000 m water depth (Kenyon et al., 2003; Mienis et al., 2006). These ridges and mounds are formed by reef building corals such as *D. pertusum* and *M. oculata* and host a variety of associated macrofauna (e.g., sponges, crinoids, and polychaetes; van Weering et al., 2003; Van Soest and Lavaleye, 2005; Duineveld et al., 2007; Mienis et al., 2009b). The seafloor around the mounds and ridges in the study area consists mostly of biogenic sandy sediment, pebbles, and boulders (Fig. 1E; Mienis et al., 2006; de Haas et al., 2009). The flanks of the ridges and mounds are covered by dead coral framework, coral rubble, and patches of living coral, whereas at the mounds summits dense populations of living corals are found (van Weering et al., 2003; De Clippele et al., 2019; Maier et al., 2021). The dominant current direction along the SE Rockall Bank margin is towards the south-west, driven by a cyclonic gyre circling the Rockall Bank (Hansen and Østerhus, 2000; Holliday et al., 2000; Mienis et al., 2007; Schulz et al., 2020). The bottom water temperature between 600 and 1000 m depth varies from 6 to 10 °C and the salinity ranges between 35.1 and 35.4 psu (Mienis et al., 2007). The bottom currents are also mainly in a south-west direction and can peak at 75 cm s^{-1} (Mienis et al., 2009a). A dominant diurnal baroclinic (internal) tide has been measured (van Haren et al., 2014) and can be seen as a modified Kelvin wave (Cyr et al., 2016), which causes cross-slope transport of water over

[1] Cruise report: 10.5281/zenodo.1454464.

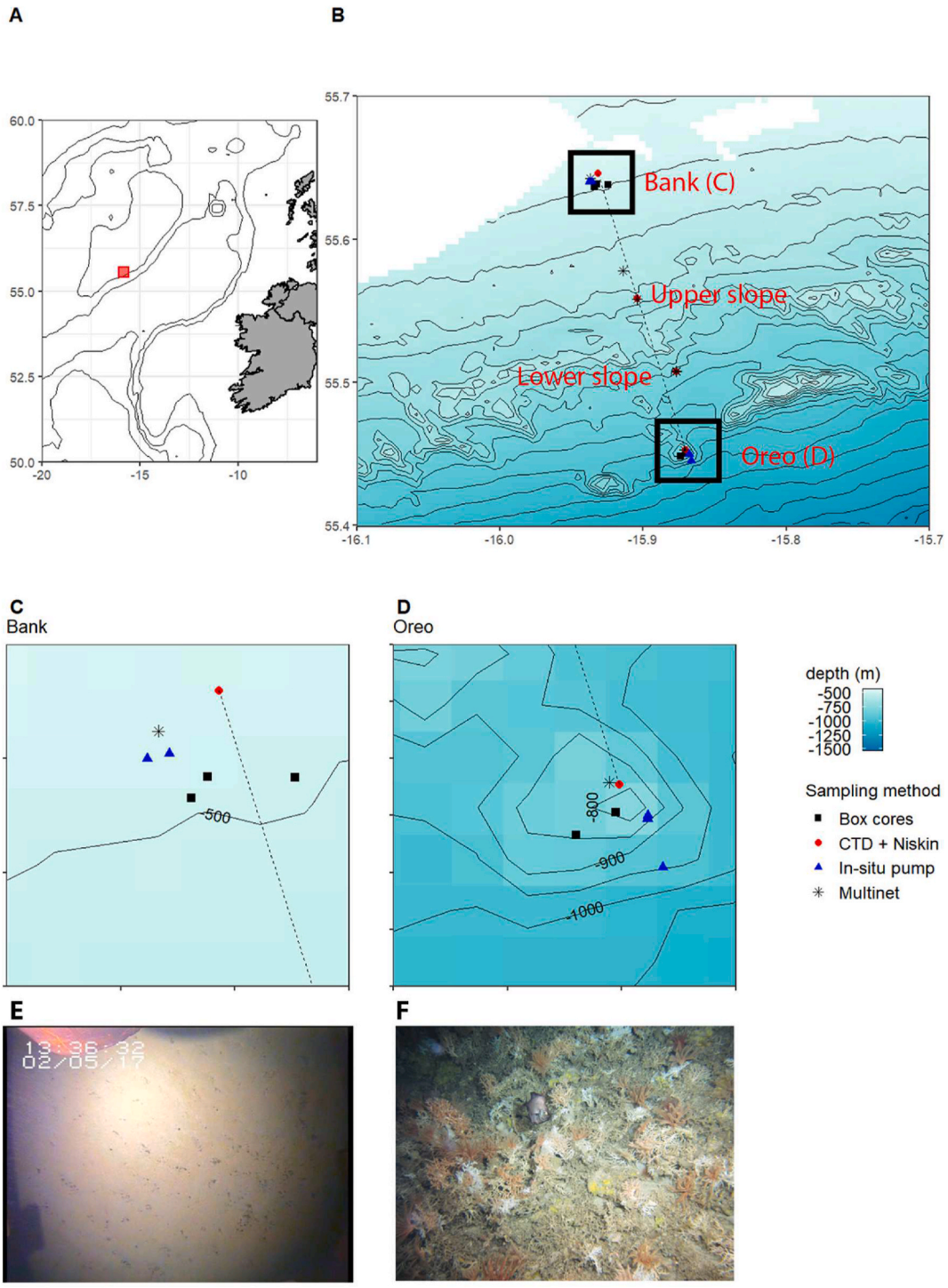

Fig. 1. *Map of the study area showing the transect of the four 24-h CTD stations, box cores, in-situ pumps, and multinet sampling locations. The length of the transect is approximately* 23 km. *A) Location of the study area in the Atlantic Ocean. B) Transect along the south-eastern slope of Rockall Bank. C) zoom-in on Bank, D) zoom-in on Oreo, E) example of seafloor at station Bank, F) example of seafloor at station Oreo. Photos are stills taken from a box core deployment video (E) and ROV footage (F). Both videos were taken during research cruise 64PE4202*F.[1] *CTD = conductivity-temperature-depth. Latitude and longitude are given in decimal degrees.*

a diurnal tidal cycle (Gerkema, 2019). Internal waves have been observed in the vicinity of these coral mounds (Huthnance, 1973; Mienis et al., 2007; Mohn et al., 2014), along with breaking of internal waves. This breaking of the wave can be caused by the interaction between the tide and the topography, and are especially predicted after the turning of the tide, which is the period of highest turbulence (van Haren et al., 2014; Cyr et al., 2016).

2.2. Sampling stations

We collected data at four different stations along a transect from a shallow part of Rockall Bank to a coral-capped carbonate mound: Bank, Upper slope, Lower slope, and Oreo (~23 km length, Fig. 1B). Data and

samples were collected during two research cruises with the R/V Pelagia, 64PE4200F[2] from April 24, 2017 to May 12, 2017 and 64PE4361F[3] from April 29, 2018 to May 10, 2018; an overview of sampling stations is given in Table 1 and Fig. 1. Station Bank (500 m depth) consists of biogenic sandy sediments located in a sediment wave field (Fig. 1E). Upper slope (662 m depth) also consists of biogenic sandy sediments and lies north of a small mound cluster. Lower slope (843 m depth) has also biogenic sandy sediment as substrate type, and is located south of a mound cluster, next to a two layered (finer) sediment-filled area. Oreo is a carbonate mound (summit 750 m depth) with a dense thriving CWC reef (Fig. 1F; Mienis et al., 2006; de Froe et al., 2019). Reef community macrofauna (box core) and organic matter samples (*in-situ* pumps) were obtained during research cruise 64PE420 (2017) at stations Bank and Oreo. CTD-yoyos were performed for 24 h at the four transect stations during cruise 64PE436 (2018), while water samples were regularly taken from Niskin bottles at five depth intervals (details below). Zooplankton samples were taken using vertical multinet deployments at the 24-h stations (Table 1) for the determination of biomass and species composition. At stations Upper slope and Lower slope, zooplankton multinets were deployed during day and at midnight. Above Oreo, an additional multinet cast was done to obtain zooplankton samples for stable isotope and fatty acid analyses.

2.2.1. 24-Hour CTD yoyo and Niskin bottles

A total of 149 CTD casts were done by yoyoing for 24 h at each of the four sampling stations with a Sea-Bird 911 plus CTD system mounted on a steel frame in the centre of a Niskin Rosette water sampling unit. The CTD system was equipped with sensors for oxygen (SBE43), and a combined sensor for turbidity and fluorescence (Wetlabs ECO-FLNTU). Data were obtained at 24 Hz, averaged to a resolution of 1 dbar using SBE Seasave software, and only downcasts profiles were used in analysis.

At 4-h intervals, *i.e.,* seven times during the 24-h cycle, water was sampled by Niskin bottles during the CTD upcast at 5 m above bottom (mab), 50 mab, mid-water, the deep chlorophyll maximum (DCM), and 5 m below the surface. Water samples were collected for nutrient concentration, DOC concentration, bacteria, virus, and phytoplankton cell densities, suspended particulate matter (SPM), sPOM (suspended + sinking POM), and pigment concentrations. On retrieval of the Niskin bottles, water was transferred into 10 L-containers using a silicone tube and moved to a temperature-controlled room (7–9 °C) for further processing.

Nutrient samples (10 mL-syringe) were filtered over a 0.45 μm-mixed cellulose ester filter into 5 mL-pony vials and subsequently frozen at −20 °C until analysis in the laboratory at NIOZ, the Netherlands. DOC samples were taken with a pre-rinsed 20 mL-glass syringe over a pre-combusted glass fibre filter (GF/F pore size 0.7 μm; Whatman, GE Healthcare Life Sciences) into 4 mL-glass vials and stored at −20 °C. Samples for flow-cytometric cell counts of (a) bacteria and viruses, and (b) phytoplankton were taken with a 10 mL-syringe. Bacteria-virus samples were placed into 4 mL-cryo vials and fixed with glutaraldehyde (final conc. 0.5%), while phytoplankton samples were placed into a 8 mL-cryo vial and fixed with 18% hexamine-buffered formaldehyde (final conc. 1%). After cooling for 30 min at 4 °C, the flow cytometry samples were flash frozen in liquid nitrogen and stored at −80 °C. The sPOM and pigment samples were taken by filtering 3–5 L of water using a vacuum pump system. Prior to filtering, the 10 L-water container was mixed gently to ensure a uniform distribution of the particulates. The sPOM samples were filtered over a pre-weighed and pre-combusted 0.7 μm-pore size GF/F filter (diameter 47 mm). The filters were then rinsed with approximately 10 mL of an ammonium carbonate solution, stored frozen at −20 °C in a closed Petri dish until analysis. Pigment samples were filtered over a GF6 filter (47 mm), wrapped in aluminium foil, flash frozen in liquid nitrogen, and stored at −80 °C.

2.2.2. Multinet zooplankton sampling

Zooplankton samples, both for biomass and stable isotope analysis, were collected by towing a Hydrobios Multinet system (net opening 0.25 m^2) from 10 mab to the surface (100 μm mesh size, speed ~30 m min^{-1}). The multinet sampled at five depth intervals: 10 mab to 50 mab, 50 mab to 100 mab, 100 mab to 100 m depth, 100 m depth to 50 m depth, and 50 m depth to the surface. Samples for zooplankton biomass were fixed in 37% borax-buffered formalin (final conc. 4%). Samples for zooplankton stable isotope and fatty acid analyses were separated in four size fractions by serial sieving on-board: 100–200 μm, 200–400 μm, 400–1000 μm, and >1000 μm, and stored frozen (−80 °C).

2.2.3. Particulate organic matter sampling with in-situ pumps

sPOM *in-situ* pump samples were taken with a McLane Large Volume Water Transfer System Sampler (WTS-LV) *in-situ* pump (McLane Research Laboratories Inc., East Falmouth, MA, USA). Samples were taken at three depths: close to the seafloor (20 mab), at 120 mab, and at 15 m water depth. Each pump was programmed using Crosscut Version 1.0.3 for Windows before deployment. The sample volume was set to 2000 L with an initial flow rate of 7 L min^{-1}. After 50 min of filtering, the flow rate was automatically set by Crosscut to 4 L min^{-1} and at a time limit of 4 h. The *in-situ* pumps filtered up to 1400 L of water through an acid-washed 53 μm nylon mesh above a pre-combusted (400 °C; 12 h) 0.7 μm- GF/F filter. Immediately after pump retrieval, the GF/F was photographed and stored at −20 °C. Larger particles (>53 μm) collected on the nylon mesh were collected by vacuum-filtration using an additional pre-combusted GF/F and stored at −20 °C.

2.2.4. Box cores benthic fauna sampling

Benthic macrofauna were collected using a cylindric box core (diameter: 50 cm, height: 55 cm, sampling area: ~0.2 m^2) as described in de Froe et al. (2019). Benthic macrofauna were sorted on-board into broad taxonomic groups and stored frozen upon analysis (−20 °C).

2.3. Laboratory analyses

2.3.1. Nutrients, DOC, sPOM, and plankton

Nutrient samples were analysed using a SEAL QuAATro analyser (SEAL Analytical Inc.) following standard colorimetric procedures. Water samples for DOC concentration were measured by automated UV-wet oxidation to CO_2 using a Formacs^{HT} Low Temperature Total Organic Carbon Analyser in combination with a non-dispersive infrared detector (Skalar). Unfortunately, concentration of NH_4^- could not be determined accurately due to a technical error.

sPOM samples were freeze-dried, weighed, and analysed for organic carbon content, total nitrogen content, and organic carbon isotopic composition ($\delta^{13}C$) using an elemental analyser (Flash 1112, THERMO Electron Corporation) coupled to an isotope ratio mass spectrometer (EA-IRMS, DELTA-V, THERMO Electron Corporation). Pigment samples were first freeze-dried, then extracted with 90% acetone (Wright et al., 1991), and subsequently quantified by high performance liquid chromatography in combination with a fluorescence detector and a photodiode array absorption detector (Zapata et al., 2000).

Phytoplankton flow cytometry samples were analysed on a BD FACS Canto II flow cytometer (Becton Dickinson, San Jose, California) equipped with a 488 nm argon laser (Brussaard et al., 2013). Based on autofluorescence and sideward scatter signal, we distinguished four phytoplankton groups: nano-eukaryotes (NEUK), cryptophytes (CRYP), pico-eukaryotes (PEUK), and cyanobacteria (CYANO). The bacterial and viral samples were analysed using a BD FACS Calibur following the protocol of Marie et al. (1999) and Brussaard (2004). Samples were diluted with a Tris-EDTA (TE) buffer and subsequently stained with SYBR Green I (Molecular Probes, Invitrogen Inc.). Based on green

[2] Cruise report: 10.5281/zenodo.1454464.
[3] Cruise report: 10.5281/zenodo.1454096.

Table 1
Overview of sampling stations. Latitude and longitude coordinates are displayed in decimal degrees. * = averaged depth of all samples, n = number of samples. Number of Niskin bottles are total number of bottles from all depths combined. SI = stable istotopes.

Sampling	Station	Date	Cruise	Lat	Lon	Depth (m)*	n
In-situ pump system	Bank	3 May '17	64PE420	55.64	−15.94	470	3
"	Oreo	7 May '17	64PE420	55.45	−15.87	740	3
Box core	Bank	30 April '17	64PE420	55.64	−15.93	503	3
"	Oreo	4 May '17	64PE420	55.45	−15.87	838	2
CTD yoyos	Bank	3–4 May '18	64PE436	55.65	−15.93	486	53 casts
"	Upper slope	4–5 May '18	64PE436	55.56	−15.90	662	39 casts
"	Lower slope	5–6 May '18	64PE436	55.51	−15.88	843	25 casts
"	Oreo	2–3 May '18	64PE436	55.45	−15.87	757	33 casts
Niskin	Bank	3–4 May '18	64PE436	55.65	−15.93	486	35 bottles
"	Upper slope	4–5 May '18	64PE436	55.56	−15.90	662	35 bottles
"	Lower slope	5–6 May '18	64PE436	55.51	−15.88	843	30 bottles
"	Oreo	2–3 May '18	64PE436	55.45	−15.87	757	35 bottles
Multinet zooplankton	Bank	3–4 May '18	64PE436	55.64	−15.94	482	5 (day)
"	Upper slope	4–5 May '18	64PE436	55.56	−15.90	659	10 (day/night)
"	Lower slope	5–6 May '18	64PE436	55.51	−15.88	844	10 (day/night)
"	Oreo	2–3 May '18	64PE436	55.45	−15.87	755	10 (biomass/SI)

fluorescence versus sideward scatter signal, we distinguished two groups of bacteria: high DNA containing bacteria (HBAC) and low DNA containing bacteria (LBAC) and three virus groups (vir I, vir II, and vir III). Final measured counts of cells/virions were corrected for a blank containing only TE-buffer and SYBR-Green I prepared and analysed using the same procedure as the samples. Gate settings and an example plot can be found in the supplementary material (Fig. S9).

2.3.2. Benthic macrofauna and zooplankton

Individual copepods were counted, and the species/genera, stage, and sex were identified by the Institute of Oceanology in Gdansk, Poland (www.iopan.pl). Prosome length was measured for 10 individuals in each species/stage group in all samples. Non-copepod zooplankton groups were identified to genus or species level and counted; their total length was measured.

Benthic macrofauna and zooplankton samples were freeze dried and ground with a pestle and mortar or ball mill to homogenize the samples (list of samples: supplements Table 5). Subsamples (CWCs ± 20–30 mg, sponges ± 10 mg, ophiuroids, crinoids, and bivalves ± 2 mg) were transferred into silver cups. Carbonate-containing samples were exposed to hydrochloric acid fume (37% HCL) for three days and subsequently acidified in a by drop-wise addition of dilute HCl (2%, 5%, and 30%) prior to analysis. Samples were analysed for organic carbon content, total nitrogen content, and $\delta^{13}C$ and $\delta^{15}N$ on an Elemental Analyser coupled to an Isotope Ratio Mass Spectrometer (EA-IRMS, Thermo flash EA 1112). The $\delta^{13}C$ and $\delta^{15}N$ isotope values are expressed in parts per thousand (‰) relative to the Vienna Pee Dee Belemnite (VPDB) standard and atmospheric nitrogen, respectively.

Total lipids were extracted from macrofauna samples (6 mg–1 g) with a modified Bligh & Dyer method, incubating the samples in a mix of methanol and chloroform (2 : 1) for 2 h at room temperature (Boschker et al., 1999; Maier et al., 2019). The lipid-containing chloroform extract was separated by polarity into neutral-lipid derived fatty acids (NLFAs) and phospholipid-derived fatty acids (PLFAs) over a silicic acid (Merck) column, then derivatised by mild alkaline methanolysis to fatty acid methyl esters (FAMEs). The respective NLFA/PLFA FAMEs were separated using gas chromatography (GC, HP G1530) on a BPX70 column (SGE Analytical Science) coupled to a Flame Ionization Detector (GC-FID) Trace GC Ultra.

2.3.3. Particulate organic matter sampled by in-situ pumps

The *in-situ* pump sPOM samples were freeze-dried and circles (10 mm diameter <53 μm; 4 mm diameter >53 μm) were punched out from the GF/F filters as subsamples to measure the content of particulate organic carbon (POC, n = 2) and particulate nitrogen (PN, n = 2). POC samples were de-carbonised prior to analysis (Yamamuro and Kayanne, 1995). POC and PN content was measured on a Thermo Scientific FlashSmart Elemental Analyser. $\partial^{13}C$ and $\partial^{15}N$ of POC and PN were determined on separate punches using an EA-IRMS (COSTECH EA and Delta 5-Advance MS, Thermo-Fisher Scientific). Lipids were extracted following a modified method described in Wolff et al. (1995). In short, sPOM samples were placed in a glass extraction thimble, an internal standard (100 μL of 5α(H)-cholestane; 101 ng μL^{-1}) was added followed by a mixture of dichloromethane and methanol (9:1; 15 mL). The extract was evaporated to dryness under a vacuum, passed through anhydrous sodium sulphate, dried under N_2 gas, and stored (−20 °C). Samples were then transmethylated (10% acetyl chloride/methanol; Christie, 1982), passed through a Pasteur pipette potassium carbonate column, and finally derivatised with N,O-Bis(trimethylsilyl)trifluoroacetamide (BSTFA; 30 μL, 40 °C, 30 min), blown down under N_2, and stored (−20 °C) until analysis by gas chromatography-mass spectrometry (GC-MS). Mass data were collected at a resolution of 600 Da, cycling every second from 50 to 600 Da, and were processed using Xcalibur software. The relative response factors of the analytes were determined individually for 36 representative fatty acids, sterols, and an alkenone using authentic standards. Response factors for analytes where standards were unavailable were assumed to be identical to those from available compounds of the same compound class.

2.4. Data analysis

2.4.1. Partitioning the total particulate organic carbon

To estimate the composition of POC for the 24-h sampling stations, each of the following components was quantified. Phytoplankton/bacteria/virus cell/particle density, measured by flow cytometry, was multiplied by a cell/particle-to-carbon conversion factor taken from literature (Supplements Table 6). Total phytoplankton C stock was calculated by multiplying the chlorophyll-*a* (chl-*a*) concentration with 40 (de Jonge, 1980). Conversion factors for nanoplankton are uncertain (Ribeiro et al., 2016). Our data consisted of two nanoplankton phototrophic groups (NEUK and CRYP) and two picoplankton phototrophic groups (PEUK and CYANO). Carbon content for CRYP range from 23 to 83 pg C $cell^{-1}$ (i.e. Berggreen et al., 1988; Tarran et al., 2006; Verity et al., 1992). Casey et al. (2013) reported a conversion factor of 2–6 pg C $cell^{-1}$ for eukaryotic phytoplankton, but it is not clear whether PEUK or NEUK were studied. In addition, the sampling location of phytoplankton is also important as cells tend to be smaller in tropical waters compared to temperate regions. We decided to use 50 pg C $cell^{-1}$ for both the CRYP and NEUK groups, 2590 fg C $cell^{-1}$ for PEUK, and 255 fg C $cell^{-1}$ for CYANO. Remaining phytoplankton (i.e. diatoms) C stock was calculated as total phytoplankton stock minus the sum of nanophytoplankton and picophytoplankton. The biomass of bacterioplankton was estimated at

20 fg C cell^{-1} for both HBAC and LBAC (Lee and Fuhrman, 1987; Ribeiro et al., 2016). We used a viral particle-to-carbon conversion factor of 0.2 fg C particle^{-1} (Suttle, 2005). Biomass of copepods and other zooplankton was calculated using length:carbon-weight regressions from literature (see Tables 1 and 2 in Middelbo et al., 2018; and i.e., Klein Breteler, 1982; Hirche and Mumm, 1992; Sabatini and Kiørboe, 1994; Satapoomin, 1999; Hygum et al., 2000; Madsen et al., 2001). Lastly, the total zooplankton carbon stock was obtained by summing all species/specimens.

The relative contribution of each C stock was obtained via division by POC concentration. The total measured POC concentration minus the sum of phyto-, bacterio, and zooplankton-C stock was then classified as 'detritus'. Here, we assume that the GF/F filter retained the majority of sPOM present in the water, except for viruses. While some studies indicate that a substantial number of bacteria can pass through the GF/F filter used for measuring POC (up to 30% of bacterial biomass; Altabet, 1990), others found a minor effect (<10% of bacteria passing the filter; Caron et al., 1995). As we calculated bacterial/picophytoplankton C stock from cell counts, the bacterial/picophytoplankton fraction, and thereby the live POC fraction, is likely slightly overestimated in our results. However, this did not affect biomass and cell density estimates of bacteria and picophytoplankton. Furthermore, the viral C stock was divided by POC concentration, but is not accounted in measured detrital POC since viruses do pass through the GF/F filters. The Niskin bottle samples and zooplankton were taken over different timescales and quantities. Therefore, we only used POC and plankton concentrations averaged over the 24-h cycle.

2.4.2. Organic matter quality indices

Common proxies for organic matter quality in the water column were used. We measured the chlorophyll-a:∑phaeopigment ratio (Lavaleye et al., 2002), where a higher value indicates relatively fresher material. We refer to ∑phaeopigments as the sum of phaeophytin and phaeophorbide. We also measured the C/N ratio of sPOM, where high values suggest relatively more reworked material and the polyunsaturated fatty acid/monounsaturated fatty acid (PUFA/MUFA) ratio, where higher values suggest relatively fresher material (Kiriakoulakis et al., 2007).

2.4.3. Trophic markers to food sources for benthic communities

To identify potential food sources for the benthic macrofauna, we used stable isotopes and fatty acid/lipid trophic markers. The $\delta^{13}C$ and $\delta^{15}N$ composition of sPOM, zooplankton, and macrofauna were analysed using biplots, and differences between groups were statistically tested with Kruskal-Wallis and Dunn's tests. We did not correct $\delta^{13}C$ values for lipid-$\delta^{13}C$, as this is unusual on deep-sea invertebrates (i.e., Iken et al., 2001; Fanelli et al., 2011b, 2011a; van Oevelen et al., 2018). For benthic macrofauna and zooplankton samples, we used fatty acid trophic markers (FATM) to indicate the consumption of zooplankton, phytoplankton, and bacteria (supplements Table 7;e.g. Dalsgaard et al., 2003). For *in-situ* sPOM samples, we used total lipid trophic markers (including alcohols and sterols) to estimate the relative contribution of zooplankton, phytoplankton, and bacteria to the sPOM composition (supplements Table S8). To investigate if sPOM is dominated by diatom or dinoflagellate cells, we also calculated the ratio between $C_{20:5\omega3}$ (eicosapentaenoic acid or EPA), and $C_{22:6\omega9}$ (docosahexaenoic acid or DHA). A high EPA/DHA ratio is generally found in diatoms, while a low ratio is found in dinoflagellates (Dalsgaard et al., 2003).

2.4.4. Tidal model

Barotropic tidal components were estimated with a tidal model to determine the phase and magnitude of the barotropic tidal cycle for each CTD cast. The principal semi-diurnal (M2) and diurnal (K1) harmonics of barotropic tidal currents were extracted from the regional Atlantic Ocean 2011-atlas solution of the Oregon State University Tidal Inversion Software (OTIS; Egbert and Erofeeva, 2002). Atlantic Ocean 2011-atlas is based on a regional 1/12° Atlantic Ocean solution in deep water incorporating high resolution local solutions in a number of coastal areas. Tidal components (M2 and K1) were combined (supplements Fig. S10) and presented for the same period as the 24-h CTD stations.

2.4.5. Data reporting and statistical tests

Data are reported as mean ± standard deviation. Data were analysed

Table 2
Summary statistics (mean ± standard deviation) for surface water and bottom water samples at the four 24-h stations for SPM, POC, DOC, and zooplankton (ZP). Letters (a, b) represent statistical groups and indicate which stations were statistically different, where "a" has a higher median than "b". "ab" means the group is not statistical different from group a, and group b. Differences were significant if p value ≤ 0.05. Krus = Kruskall-Wallis test, Dunn = Dunn's test. * Upper value = Niskin bottles, lower value = in-situ pumps. Colour fills are coherent with the statistical groups, to visualize difference between stations.

	Variable	Test	Bank	Upper slope	Lower slope	Oreo
Surface	SPM (mg L^{-1})	Krus	3.2 ± 1.4^{a}	3.2 ± 1.0^{a}	3.6 ± 0.8^{a}	3.1 ± 0.8^{a}
	POC (μM)*	Dunn	16.9 ± 3.4^{a} / 1.1 ± 0.8	17.9 ± 6.4^{a} / -	12.4 ± 3.7^{ab} / -	9.6 ± 3.7^{b} / 2.9 ± 2.6
	DOC (μM)	Krus	93 ± 23^{a}	97 ± 24^{a}	87 ± 17^{a}	116 ± 73^{a}
	ZP (mmol C m^{-3})	Krus	1.1 ± 0.4^{a}	0.7 ± 0.3^{a}	0.6 ± 0.2^{a}	0.5 ± -^{a}
Bottom	SPM (mg L$^{-1)}$	Krus	2.1 ± 0.6^{a}	2.3 ± 0.9^{a}	2.7 ± 0.6^{a}	2.5 ± 0.6^{a}
	POC (μM)*	Dunn	2.3 ± 0.8^{a} / 1.3 ± 0.8	2.1 ± 0.8^{a} / -	1.8 ± 0.6^{a} / -	1.8 ± 0.9^{a} / 0.3 ± 0.1
	DOC (μM)	Krus	92 ± 19^{a}	88 ± 31^{a}	76 ± 20^{a}	128 ± 87^{a}
	ZP (mmol C m^{-3})	Krus	0.05 ± 0.01^{a}	0.02 ± 0.01^{a}	0.02 ± 0.02^{a}	0.01 ± 0.00^{a}

in statistical software program R (R Core Team, 2019), and the R packages: *plot3D*, *OceanView*, *reshape2*, *RNetCDF*, *readxl*, *knitr*, *rmarkdown*, *ggplot2*, *cowplot*, *patchwork*, *oce*, *lubridate*, *dplyr*, *akima*, *FSA*, *RColorBrewer* (Wickham, 2007, 2016, 2; Grolemund and Wickham, 2011; Neuwirth, 2014; Michna and Woods, 2019; Soetaert, 2019b, 2019a; Wickham and Bryan, 2019; Wilke, 2019; Akima and Gebhardt, 2020; Kelley and Richards, 2020; Xie, 2020; Allaire et al., 2021; Ogle et al., 2021; Wickham et al., 2021). Parameter differences between stations were tested for both surface and bottom waters. To increase the statistical power, we pooled the 5 m and deep-chlorophyll maximum samples together for surface waters, and the 50 mab and 5 mab samples for bottom waters. The significance of spatial and temporal differences were first tested for normality with the Shapiro-Wilk test, and subsequently by ANOVA combined with a Tukey's HSD test with normally distributed data and by a non-parametric Kruskal-Wallis test combined with Dunn's test for non-normally distributed data. Lipid concentrations were converted to mole% and transformed by subtracting the mean for each compound. Lipid composition of *in-situ* pump sPOM was analysed by principal component analysis (PCA) and analysis of similarities (ANOSIM) on differences between sites and size classes.

3. Results

3.1. Physical and biogeochemical water-column characteristics during a tidal cycle

Bottom temperature at station Bank showed a semi-diurnal pattern with an amplitude of 20–50 m (Fig. 2A). Temperature profiles revealed a diurnal tidal cycle with an amplitude of 50–100 m at the Upper slope and of 150–200 m at the Lower slope and Oreo (Fig. 2B–D) at ~400 m depth. In addition, at Lower slope, an overturning event was apparent just below the DCM, which transported water from 50 to 300 m depth (supplements Fig. S11C). At Oreo, a higher frequency (~6 h) tidal signal was recorded by the CTD casts superimposed on the diurnal pattern with an amplitude of 200 m (Fig. 2C). Bottom water temperatures dynamics at the four stations corresponded well with the barotropic tidal current speed and direction (Fig. 2E–H); when the tidal current speed increased in a northward direction, the bottom water temperature dropped, indicating that colder water was advected upslope, and when tidal currents turned to a southward direction, the opposite effect was seen. These temperature changes were most pronounced at Upper slope, Lower slope, and Oreo. Profiles of seawater density and buoyancy frequency showed that the water column at Bank and Lower slope was more stable than at Upper slope and Oreo (Fig. 2I–L; supplements Fig. S12). At Oreo, two water column instabilities, at 400 m and 580 m depth, were observed during the full diurnal tidal cycle (Fig. 2L), while at Lower slope this was observed at 700m depth. No such overturning was apparent at Bank and Upper slope.

Fluorescence and turbidity were the highest in the surface waters and decreased with depth at all stations. At the station Upper slope, Lower slope, and Oreo, turbidity slightly increased again between 400 m depth and the seafloor (supplements Figure S11 I-K). Silicate, nitrate, and phosphate concentrations increased with water depth at all stations (supplements Fig. S13; Fig. 5). Nutrient concentrations in surface waters were generally lower at Bank and Upper slope than at Lower slope and Oreo. For example, surface nitrate concentrations were significantly lower at Bank (7.89 ± 2.11 μM) and Upper slope (7.69 ± 0.59 μM) than at Oreo (8.73 ± 0.25 μM; TukeyHSD, $p < 0.05$). Lower slope surface

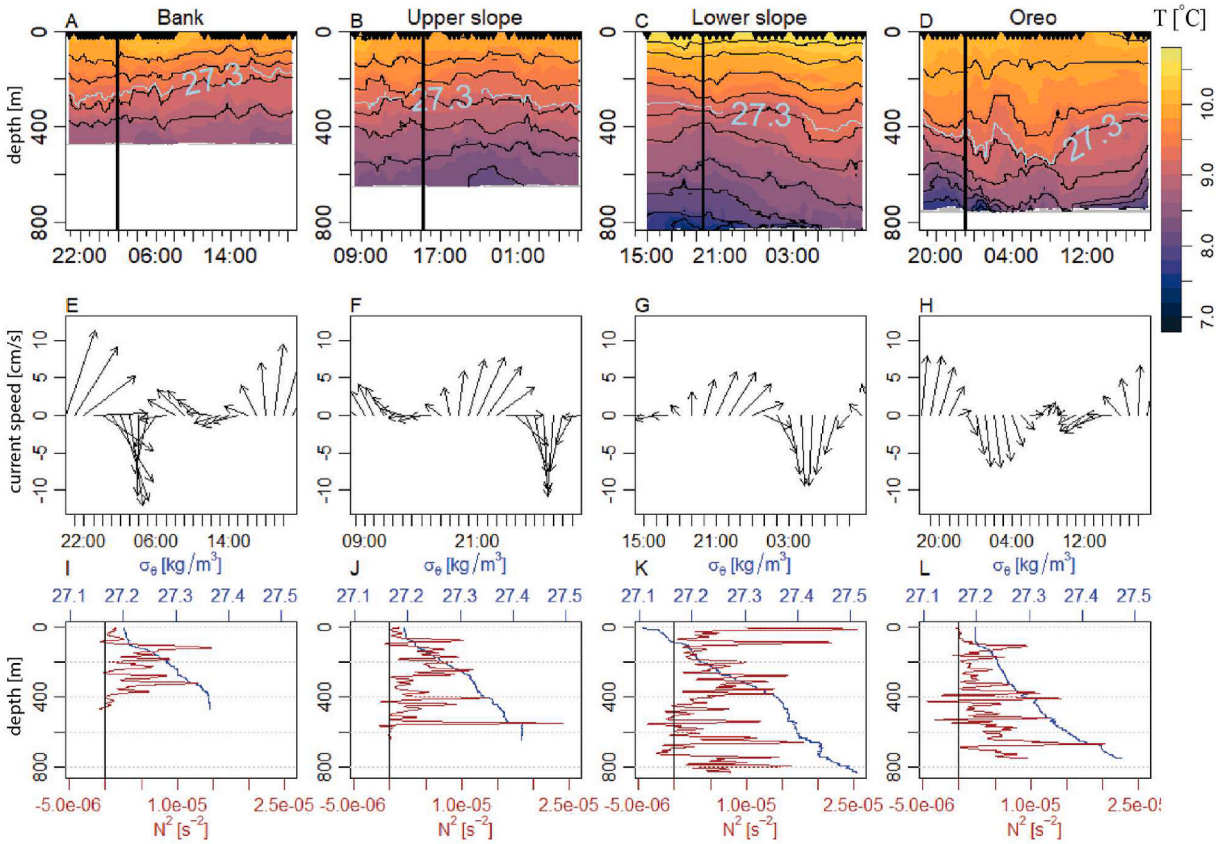

Fig. 2. Temperature profile during the tidal cycle for Bank (A), Upper slope (B), Lower slope (C), Oreo (D). The contour lines represent density with 0.04 kg m^{-3} difference between each line, and the blue line represents the 27.3 isopycnal. Temperature is expressed in °Celsius. Black triangles at the top of plots A-D show the CTD casts. Barotropic tidal (M2 and K1 combined from tidal model) current speed and direction in cm s^{-1} for Bank (E), Upper slope (F), Lower slope (G) and Oreo (H). CTD profiles of density (in blue) and Buoyancy frequency (in brown) for Bank (I), Upper slope (J), Lower slope (K) and Oreo (K). Sampling time of these CTD profiles is indicated by the black triangles at the top of figures A–D.

water showed intermediate nitrate concentrations (8.15 ± 0.55 μM). Silicate values in surface waters at Bank and Upper slope approached zero at the end of the 24-h cycle. Moreover, the silicate and nitrate concentrations in the surface waters were correlated (0.87–1.2, $R^2 >$ 0.9) at all four stations (supplements Fig. S14).

3.2. Organic matter distribution in the water column during a tidal cycle

3.2.1. Particulate and dissolved organic matter distribution

Suspended particulate matter (SPM) concentrations measured in Niskin bottles were higher in the surface (3.1–3.6 mg L^{-1}) than in bottom samples (2.1–2.7 mg L^{-1}) for all 24-h stations (Table 2; supplements

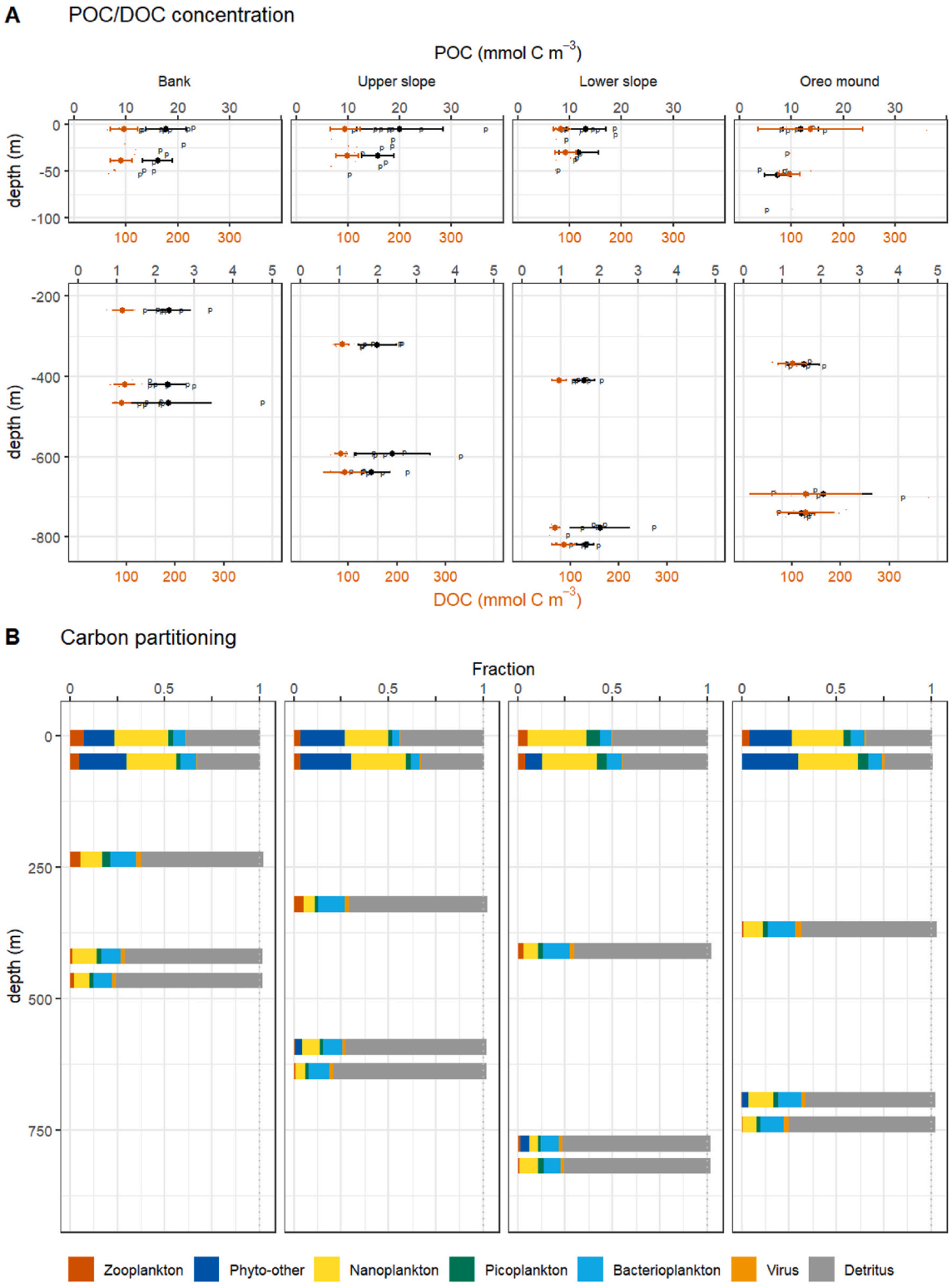

Fig. 3. A) POC (in black) and DOC (in orange) concentrations plotted over depth for the four sampling stations. Top x-axis is POC concentration, bottom x-axis indicates DOC concentration. Note the different scale for POC in the top and bottom plot of subplot to visualize bottom water differences. B) Carbon partitioning over indicated groups for the four stations.

Fig. S15). Surface water POC was significantly higher at Bank and Upper slope compared to Oreo. Fluorescence (Supplements Figs. S11E–H) and pigment concentrations (supplements Fig. S16) were likewise higher in the surface water at Bank and Upper slope compared to Lower slope and Oreo. Additionally, bottom water POC concentrations were on average higher at Bank and Upper slope than at Lower slope and Oreo ($p < 0.1$; Table 2; Fig. 3A). Surface POC concentrations measured by *in-situ* pumps were 4–20 times lower than in the Niskin bottle samples. Furthermore, the surface POC concentration at Oreo, measured by *in-situ* pumps, was higher compared to the Bank and the material consisted mostly of small sPOM (<0.53 μm). In contrast, the bottom-water POC concentration, measured by *in situ* pumps, was higher at the Bank than at Oreo and consisted mostly of large sPOM (Table 2; >0.53 μm; supplements Fig. S17). The mean surface DOC concentration was higher at Oreo compared to the other stations, but differences were not statistically significant (Table 2). Moreover, the average bottom DOC concentration was higher at Oreo as compared to Bank, Upper slope, and Lower slope (Dunn's test, $p < 0.10$). Lastly, several peaks of DOC concentration of up to 380 μM were observed in the surface and bottom water at Oreo (Fig. 3A).

3.2.2. Pigment, nano-, picoplankton, bacteria, and viruses water concentrations

Pigments in the surface water samples at the four stations were composed mostly of chl-*a* and fucoxanthin (Fig. S16). Surface water chl-*a* concentrations, averaged over the full tidal cycle, were significantly higher at the Bank and Upper slope compared to the Lower slope and Oreo (Table 3). A non-parametric Dunn's test, which compares medians, showed significantly lower values of chl-*a* concentration for the Lower slope and Oreo compared to the Bank, but average chl-*a* concentration was highest at Oreo due to large variability over the tidal cycle (Table 3). Surface water chlorophyllide-a concentration increased during the 24-h sampling period at Bank and Upper slope (Fig. S17 A & B) Nanophytoplankton consisted mainly of NEUK. Surface water showed higher concentrations of total nanoplankton (NEUK + CRYPT) at Bank than at Lower slope and Oreo (Table 3). Nanophytoplankton concentrations (NEUK + CRYPT) decreased with depth at all stations (supplements Fig. S18) and the concentration in the bottom water was significantly higher at Bank than at Upper slope and Lower slope (Table 3). Picophytoplankton comprised mostly of PEUK and CYANO and concentrations in the surface waters were significantly higher at Lower slope compared to the Bank, Upper slope, and Oreo. Picophytoplankton concentration decreased with depth (Supplement Fig. S18) and was significantly higher at Bank than at Lower slope (Table 3).

Bacterial concentrations (HBAC + LBAC) were significantly higher in the surface waters at Bank compared to the Upper slope, Lower slope, and Oreo (Table 3). The HBAC:LBAC ratio was around 1:1 for all four stations. Bottom water bacterial concentrations were elevated at the Bank compared to Lower slope. Surface and bottom water viruses were composed mainly of VirII and virIII and concentrations were higher at Bank than Lower slope (supplements Fig. S18). Viral concentrations were most variable at Oreo, with several spikes of high viral densities in the surface water ($6–8 \cdot 10^6$ particles mL^{-1}) and bottom water ($4–5 \cdot 10^6$ particles mL^{-1}), coinciding with high DOC concentrations (Fig. S20).

3.2.3. Zooplankton communities

The zooplankton community was dominated (>85% of total biomass) by calanoid copepods (primarily *Calanus* spp and *Metridia lucens*) at all stations. Zooplankton-carbon concentrations were the highest in surface waters (Table 2). Surface water zooplankton-carbon concentration (strata 0–50 m) was higher at Bank (1.4 mmol C m^{-3}) than at Lower slope (0.7/0.8 mmol C m^{-3}, day/night, respectively), Upper slope (0.5/1.0 mmol C m^{-3}, day/night), and Oreo (0.5 mmol C m^{-3}). At Upper slope, a shift in carbon concentration at 300 m depth (from 0.2 to 0.05 mmol C m^{-3}) and surface waters (from 0.5 to 1.1 mmol C m^{-3}) was observed between day and night, respectively (supplements Fig. S21). Bottom zooplankton carbon concentration was generally low, ranging from <0.01 mmol C m^{-3} at Oreo to 0.05 mmol C m^{-3} at the Bank.

3.2.4. Partitioning of particulate organic carbon

The bottom water at Oreo mound had the highest living POC fraction of bottom water at the four sampling stations (26%/37%, 5 mab/50 mab), together with the 50 mab-sample at the Bank (31%), while the lowest live POC was measured at 5 mab at the Upper slope (22%; Fig. 3B). Detritus, the non-living fraction, comprised the largest fraction of POC in deeper water, ranging from 63 to 78% in bottom waters. The nanoplankton fraction of surface POC ranged from 24% for the surface water (5m) sample at Upper slope to 35% for the DCM sample at Oreo (Fig. 3), and its contribution decreased with depth 5–15% in bottom waters. Picoplankton accounted for a small fraction of the POC throughout the water column (1%–7%) and was highest in the surface water at Lower slope (7%). Remaining phytoplankton fraction was low at Lower slope (0–10%) but ranged throughout the water column from 17% to 33% for the stations Bank, Upper slope, and Oreo. Bacterioplankton dominated the POC in deeper waters (mid water, 50 mab and 5 mab), ranging from 10% at Bank to 15% at Oreo, where it also was the largest fraction of living POC. Zooplankton carbon was a small (0–5%) fraction of the POC throughout the water column, with higher contributions in surface (2–5%) than deeper waters (0–1%). Viruses represented only a small fraction of POC throughout the water column (2–3%).

3.3. Organic matter quality along the transect

3.3.1. Organic matter quality indices

Surface water chl-*a*:∑phaeopigment ratio was on average lower at the Bank compared to the other stations, but this difference was not statistically significant (Table 4). Bottom water chl-*a*:∑phaeopigment ratio was significantly lower at Bank than at Oreo. Surface water C:N ratio of sPOM was significantly higher at Oreo than at Bank and Upper slope, while the bottom water C:N ratio of sPOM did not differ significantly between stations (Table 4), although variability was higher at Oreo compared to the other stations. In the surface water *in-situ* pump samples (small and large fraction pooled), the PUFA/MUFA ratio was not significantly different between the Bank and Oreo. The bottom water PUFA/MUFA ratio was on average higher at Oreo compared to Bank (TukeyHSD, $p < 0.1$).

3.3.2. Lipid composition from in situ pump sPOM

The lipid concentration showed a similar trend over depth as the POC and PN, with elevated values close to the sea floor at Bank, while values decreased with depth at Oreo (supplements Fig. S22). Lipids in the bottom water sPOM, for both the small fraction (0.7–53 μm) and the large fraction (>53 μm), were dominated by the fatty acid $C_{16:0}$ and PUFA and MUFA such as $C_{18:1}$, $C_{18:2}$, $C_{18:3}$, $C_{20:5\ \omega3}$ (eicosapentaenoic acid or EPA), and $C_{22:6\ \omega9}$ (docosahexaenoic acid or DHA), with minor amounts of sterols. PCA showed that the small fraction (0.7–53 μm) and the large fraction (>53 μm) separate along the PCA1 axis (ANOSIM; $r = 0.785$, $p < 0.001$; Fig. 4). This separation is driven largely by (1) a higher abundance/contribution of $C_{18:3\ (cis\text{-}6)}$ (diatom-fatty acid trophic marker) in the large particles, pointing to abundance of diatom aggregates, and (2) higher abundance/contribution of $C_{18:1}$ alcohols (zooplankton fatty-acid trophic marker). Differences along the PCA2 axis are driven primarily by (1) higher contribution of EPA + DHA for the high values, and (2) lower contribution of C_{16} alcohols. However, there was no significant difference in lipid composition of sPOM between the two stations (ANOSIM; $r = -0.0219$; $p = 0.596$). PUFA concentration in the bottom water was higher at the Bank compared to Oreo in both the large (140 ± 28 and 8 ± 4 ng L^{-1}, respectively) and small (299 ± 164 and 92 ± 37 ng L^{-1}, respectively) size fractions.

Table 3
Summary statistics (mean ± standard deviation) for surface water and bottom water samples at the four 24-h stations. Letters (a, b) represent statistical groups and indicate which stations were statistically different, where "a" has a higher median than "b". "ab" means the group is not statistical different from group a, and group b. Differences were significant if p value ≤ 0.05. Krus = Kruskall-Wallis test, Dunn = Dunn's test. * Upper value = Niskin bottles, lower value = in-situ pumps. Colour fills are coherent with the statistical groups, to visualize difference between stations. Chl-a = chlorophyll-a, nano = nanophytoplankton, pico = picophytoplankton, bact = bacteria.

	Variable	Test	Bank	Upper slope	Lower slope	Oreo
Surface	Chl-*a* (μg L^{-1})	Tukey	2.0 ± 0.4^{a}	2.2 ± 0.5^{a}	1.2 ± 0.3^{b}	1.5 ± 0.5^{b}
	Nano (· 10^3 cells mL^{-1})	Dunn	1.21 ± 0.40^{a}	1.17 ± 0.27^{ab}	0.97 ± 0.25^{b}	0.73 ± 0.37^{b}
	Pico (· 10^3 cells mL^{-1})	Dunn	2.83 ± 0.91^{b}	2.37 ± 0.44^{b}	5.80 ± 1.97^{a}	3.06 ± 1.51^{b}
	Bact (· 10^5 cells mL^{-1})	Tukey	8.0 ± 2.5^{a}	5.0 ± 1.6^{b}	5.7 ± 1.0^{b}	4.6 ± 1.5^{b}
	Virus (· 10^6 cells mL^{-1})	Dunn	6.5 ± 1.2^{a}	5.4 ± 1.5^{ab}	4.5 ± 0.6^{b}	5.5 ± 1.4^{ab}
Bottom	Chl-*a* (μg L^{-1})	- Dunn	0.04 ± 0.01 0.03 [median]^{a}	0.06 ± 0.14 0.02 [median]^{ab}	0.04 ± 0.08 0.02 [median]^{b}	0.07 ± 0.19 0.02 [median]^{b}
	Nano (· 10^3 cells mL^{-1})	Dunn	0.064 ± 0.054^{a}	0.043 ± 0.062^{b}	0.034 ± 0.039^{b}	0.054 ± 0.076^{ab}
	Pico (· 10^3 cells mL^{-1})	Dunn	0.50 ± 0.26^{a}	0.35 ± 0.07^{ab}	0.37 ± 0.31^{b}	0.42 ± 0.25^{ab}
	Bact (· 10^5 cells mL^{-1})	Dunn	1.6 ± 0.4^{a}	1.5 ± 0.4^{ab}	1.2 ± 0.4^{b}	1.6 ± 0.8^{ab}
	Virus (· 10^6 cells mL^{-1})	Dunn	3.0 ± 0.3^{a}	2.6 ± 0.7^{ab}	2.2 ± 0.6^{b}	2.8 ± 1.1^{ab}

Table 4
Organic matter quality indices of sPOM samples from the four stations along the transect. To increase statistical power, bottom samples are combined the 5 mab and 50 mab samples for Niskin bottles, and deployments at 10 mab and 120 mab for the in-situ pumps. In cases that two values are provided, upper value refers to samples from Niskin bottles and the lower value to samples from in-situ pumps. PUFA = polyunsaturated fatty acid, MUFA = monounsaturated fatty acid. Differences were considered significant if p ≤ 0.05. Letters (a, b) represent statistical groups and indicate which stations were statistically different, where "a" has a higher median than "b". "ab" means the group is not statistical different from group a, and group b. Differences were significant if p value ≤ 0.05. Krus = Kruskall-Wallis test, Dunn = Dunn's test. * Upper value = Niskin bottles, lower value = in-situ pumps. Colour fills are coherent with the statistical groups, to visualize difference between stations.

		Test	Bank	Upper slope	Lower slope	Oreo
Chl-*a*:Phaeo ratio	Surface	Krus	2.48 ± 1.74^{a}	3.25 ± 1.85^{a}	3.50 ± 2.38^{a}	3.26 ± 1.34^{a}
	Bottom	Dunn	0.58 ± 0.35^{a}	1.01 ± 1.05^{ab}	0.95 ± 0.91^{ab}	1.42 ± 1.06^{b}
C/N ratio*	Surface	Dunn	5.89 ± 0.46^{b} / 3.11 ± 1.73^{a}	5.86 ± 0.46^{b} / -	6.47 ± 0.58^{ab} / -	7.73 ± 2.84^{a} / 3.55 ± 1.04^{a}
	Bottom	Krus	7.5 ± 2.6^{a} / 5.6 ± 1.1^{a}	6.6 ± 1.8^{a} / -	7.6 ± 1.8^{a} / -	7.8 ± 4.0^{a} / 4.7 ± 0.9^{b}
PUFA/MUFA ratio	Surface	Krus	4.54 ± 4.12^{a}	-	-	1.91 ± 1.74^{a}
	Bottom	Krus	1.83 ± 0.53^{a}	-	-	2.27 ± 0.49^{a}

3.3.3. *Tidal effect and organic matter quality*

At Oreo, we observed a possible effect of an internal tidal wave on organic matter composition/quality near the coral mound seafloor. After the internal wave passed (23:00), the 50 mab water samples at Oreo (Fig. 5) showed an increase in all measured sPOM variables (i.e., POC, chl-*a*, picophytoplankton), and a decrease in nutrient concentration (Fig. 5). There was also a second peak in picophytoplankton at 22:30, with a corresponding lower nutrient concentration. Accordingly, the bottom water was more oxygen-rich and warmer after the tidal wave passed (Fig. 5 E&F, Fig. 2D&H).

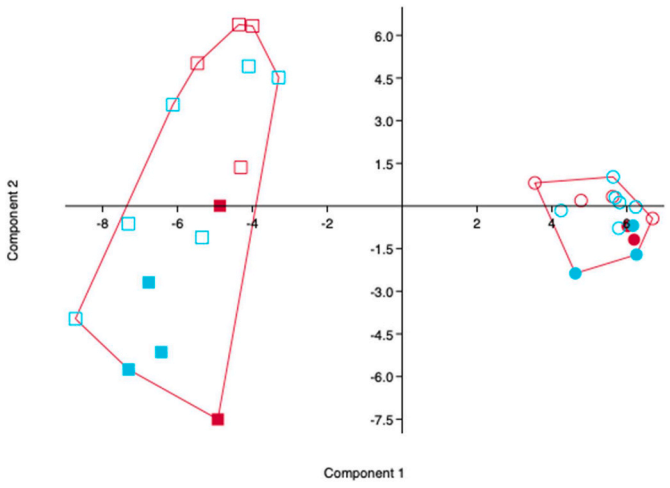

Fig. 4. sPOM lipid composition. Squares >53 μm, circles 0.7–53 μm; filled – surface, open – deep, red is Bank, cyan is Oreo. PC1 and PC2 scales show Eigenvalues.

3.4. Linking organic matter in the water column to the macrobenthos

3.4.1. Isotopes and C/N ratios of sPOM, zooplankton, and seafloor community

The POC from the *in-situ* pumps tended to have higher $\delta^{13}C$ values than the POC from the 24-h Niskin bottle-deployment. Bottom water POC collected by Niskin bottles showed a significantly higher $\delta^{13}C$ on the Bank (−23.9 ± 2.3‰) compared to Upper slope (−25.9 ± 1.4‰), and Lower slope (−26.0 ± 0.8‰). At Oreo, bottom water $\delta^{13}C$ of POC (−24.5 ± 2.9‰) was significantly higher compared to Lower slope (−26.0 ± 0.8‰; Dunn's test, $p < 0.05$). The POC collected by *in-situ* pump showed a higher $\delta^{13}C$ at Oreo than at the Bank (supplements Fig. S23, Fig. S24, and Fig. S25). Niskin bottle POC became depleted in ^{13}C with depth while the *in-situ* pump POC became enriched in ^{13}C with depth. The POC sampled by *in-situ* pump showed a similar $\delta^{15}N$ at the Bank and at Oreo in the surface and bottom waters, despite a difference of 300 m in depth for the latter (supplements Fig. S25). The large fraction sPOM showed around 1‰ lower $\delta^{15}N$ values than the small fraction.

Zooplankton $\delta^{13}C$ ranged from −26.5 and −20.5‰ and differed between the size classes (supplements Fig. S26C). Bottom-water zooplankton samples were depleted in $\delta^{13}C$ compared to surface-water samples. The $\delta^{15}N$ value of zooplankton increased with depth and showed a clear distinction between size classes (supplements Fig. S26B). The largest zooplankton (>1000 μm) in bottom samples have higher $\delta^{15}N$ values (8.0–8.5‰) than the smaller zooplankton (100–400 μm; 4.1–4.6‰). The C/N ratio of smaller zooplankton classes (100–400 μm) increased markedly with depth (supplements Fig. S26E). In contrast, the C/N ratio of the largest zooplankton class (1000 μm) stayed rather constant from surface to 50 mab but was increased at the bottom.

The $\delta^{13}C$ of sediment and benthic macrofauna at the Bank ranged from −23.9 to −19.1‰ and at Oreo from −22.9 to −13.2‰. The surface sediment (0–1 cm) at Oreo was on average higher in $\delta^{13}C$ (−20.6 ± 0.3‰) than the sediment at the Bank (−22.0 ± 1.2‰), but the differences were not statistically significant (ANOVA, $p > 0.05$). Likewise, bivalves showed a higher $\delta^{13}C$ at Oreo (−16.3‰) compared to the Bank (−19.7 ± 0.4‰). The sediment was higher in $\delta^{15}N$ at Bank (5.3 ± 0.4‰) compared to Oreo (4.9 ± 0.4‰), but this difference was not significant (ANOVA, $p > 0.05$). Bivalves at the Bank had a similar $\delta^{15}N$ as the sediment and were enriched in ^{15}N by 2.6‰ relative to sPOM. The $\delta^{15}N$ value of framework building CWCs (~8.0‰) were significantly enriched compared to the *in-situ* pump sPOM samples (3.0‰). Ophiuroidea, *E. norvegica*, and sponges showed the highest $\delta^{15}N$ and $\delta^{13}C$ values overall (Fig. 6B).

3.4.2. Fatty acids/lipids of suspended and seafloor communities

Phytoplankton biomarkers were the largest fraction of sPOM lipids throughout the water column and at both sites (Bank, bottom-water: 44.9 ± 12.0% of lipids; Oreo, bottom-water: 44.0 ± 9.3% of lipids). Bacterial and zooplankton biomarkers in bottom sPOM samples were on average higher at the Bank (1.6 ± 0.5% and 21.1 ± 7.6% of lipids, respectively) than at Oreo (1.0 ± 0.4% and 16.9 ± 6.4% of lipids, respectively), but the differences were not significant (Kruskall, $p > 0.05$). Zooplankton lipids were consistently higher in the small fraction sPOM than the large fraction (Fig. 7 A & B), and zooplankton lipids in sPOM increased with depth, especially at Oreo (Fig. 7B).

Phytoplankton FATM were higher in the PLFA fraction of benthic organisms compared to the NLFA fraction, except for *E. norvegica*. The macrofauna *M. oculata*, *E. norvegica,* and Ophiuroidea contained more zooplankton FATM in their PLFA pool compared to Stylasteridae. Zooplankton in bottom-waters contained mostly FATM for zooplankton and phytoplankton (Fig. 7C and D). Sponges showed higher bacterial FATM in their NLFA pool compared to the other benthic organisms. In addition, the EPA/DHA ratio of sPOM differed between the small (0.7–53 μm) and the large (>53 μm) fraction (supplements Fig. S27). The small sPOM fraction had an EPA/DHA ratio between 0.8 and 1.2, indicating no specific domination by any one phytoplankton group. The large sPOM fraction showed mostly an EPA/DHA ratio above 1, which suggests that the phytoplankton community is dominated by diatom cells. The CWCs had an EPA/DHA ratio above 1 in the NLFA fraction, but <1 in the PLFA fraction. The bivalve sample from the Bank station showed an EPA/DHA ratio close to zero in both the NLFA and PLFA fractions, indicating a dinoflagellate-rich diet. DHA was not detectable in most zooplankton samples.

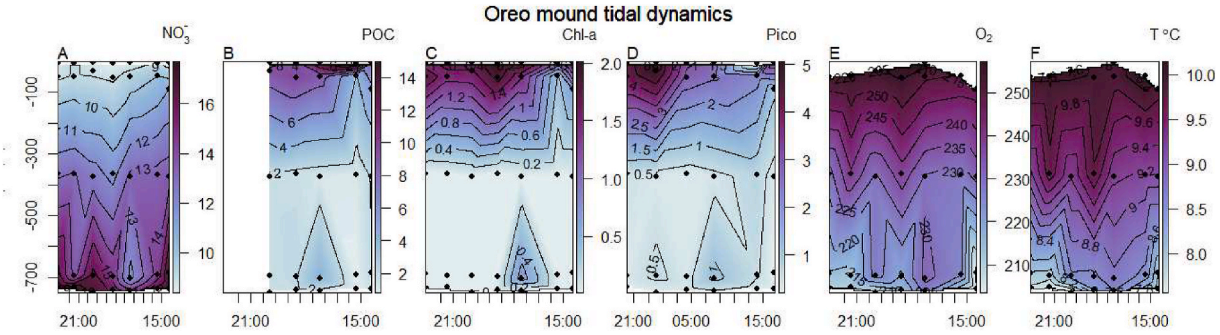

Fig. 5. Interpolated profiles of Oreo mound during a tidal cycle with A) Nitrate concentration in μM, B) particulate organic carbon concentration in μM, C) chl-a concentration in μg L^{-1}, D) total picophytoplankton concentration in · 10^3 cells mL^{-1}, E) oxygen concentration in μmol L^{-1}, and F) temperature in degrees Celsius. The x axis shows sampling time, the y axis shows depth in metres. Note that the first two samples for POC were not available due to a sampling error.

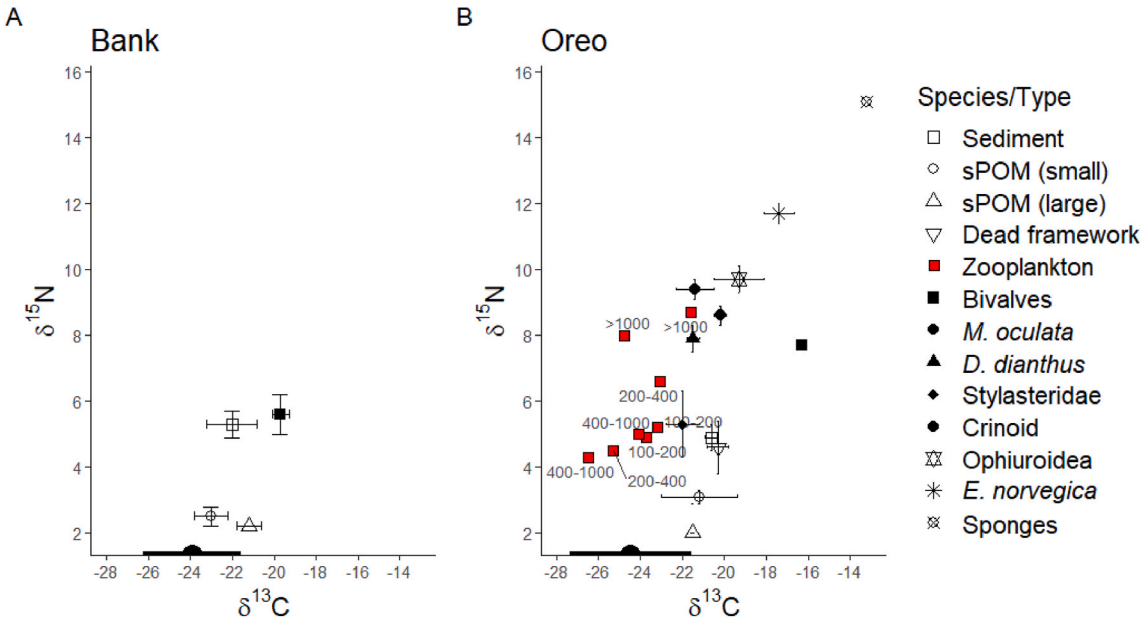

Fig. 6. $\delta^{13}C$ and $\delta^{15}N$ stable isotope biplots for stations Bank (A) and Oreo (B). Size classes of zooplankton are shown inside the plot area (e.g., 400–1000 μm). sPOM samples, both small and large, are from the in-situ pump system. Niskin bottle sPOM $\delta^{13}C$ values (no $\delta^{15}N$ data available) are shown on the x-axis. Only bottom water sPOM and zooplankton are included in the plot.

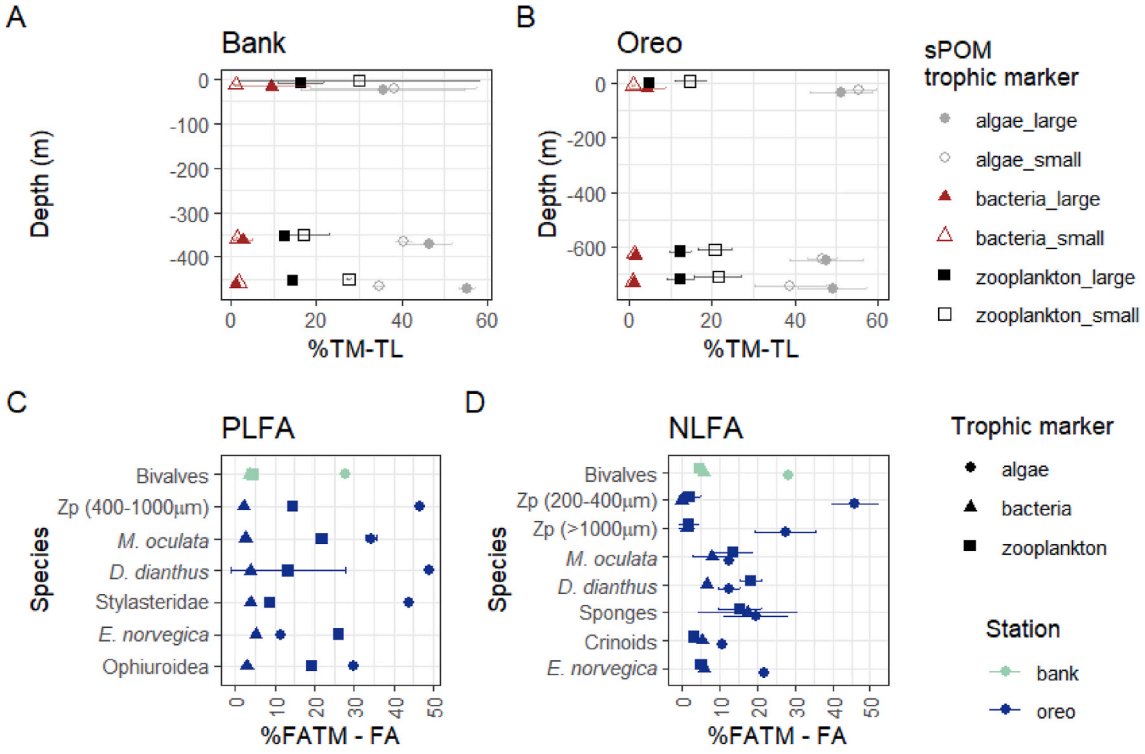

Fig. 7. Lipid trophic markers of total lipids in the sPOM (small – and large fraction separately) at A) Bank and B) Oreo. %TM-TL = percentage trophic marker of total lipids. C) Fatty acid trophic markers in phospholipid-derived fatty acids (PLFAs) in benthos D) Fatty acid trophic markers in neutral-lipid derived fatty acids (NLFA) in benthos. Zp = zooplankton. Benthos species differ between the PLFA fraction and the NLFA fraction due to a technical error in the laboratory and a limited number of available samples, therefore not all macrofauna groups present in PLFA data are present in the NLFA data, and viceversa.

4. Discussion

We attempted to gain a better understanding of the transport and availability of organic matter during a full tidal cycle above a CWC mound and the subsequent utilization of this organic matter by benthic macrofauna. In the following sections, we discuss (1) water column dynamics, (2) surface phytoplankton communities, (3) organic matter supply and quality at the coral mound, (4) organic matter distribution in the water column, and (5) the relevance of different organic matter sources as food for the benthic communities.

4.1. Water column dynamics on the south-eastern slope of Rockall Bank

Coral mounds are often found in areas with increased internal tidal activity (Mohn et al., 2014; van der Kaaden et al., 2021). The interaction between the barotropic tide and bottom topography can cause energetic hydrodynamic features, e.g., hydraulic jumps and internal bores (Hosegood and van Haren, 2004; Juva et al., 2020). Coral presence and coral mound growth is likewise linked to the combined presence of an intermediate water layer and high internal wave activity (e.g. Raddatz et al., 2014; Rüggeberg et al., 2016). We measured a relatively small (50 m) amplitude tidal wave at 400 m depth on the Bank, but a larger amplitude wave (100–200 m) with a period of approximately 24 h on the other three stations (Fig. 2A–D). This is consistent with earlier 24-h CTD yoyos performed in the area (Mienis et al., 2007). We recorded an internal wave at Oreo (~400 m depth) with an amplitude of 200 m (Fig. 2D; Fig. 5; Fig. 8, process 2a). This wave passed by after the turn of the tide and likely formed by the interaction between the barotropic tide and coral mound topography (Cyr et al., 2016). Alternatively, it could be a freely propagating internal wave, which are common in this area (Mohn et al., 2014).

Furthermore, coral growth and flourishing CWC reefs in the NE Atlantic have also been linked to a steep density gradient in a short bathymetric range and a narrow density envelope of sigma-theta (σ_Θ) = 27.35–27.65 kg m^{-3} (Dullo et al., 2008). Here, density of the bottom water at Oreo falls within this proposed envelope and shows a steep density gradient at times during the 24-h tidal cycle (Figure S12 D). Our temperature-salinity data indicate the presence of Wyville Thompson Overflow Water (WTOW) below 600 m at Oreo (see Schulz et al., 2020). The WTOW is a water mass that is considered crucial for CWC presence on the slopes of Rockall Bank, transporting food, nutrients, and coral larvae to the seafloor (Johnson et al., 2010; Schulz et al., 2020). Schulz et al. (2020) note that sPOM in WTOW is of low quality, and that it is therefore unlikely that WTOW provides food directly. Indeed, our results also show high quality sPOM was mostly present in water with a density of $\sigma > 27.4$ kg m^{-3}, which is beyond the upper density limit of WTOW (Johnson et al., 2010, 2017). Therefore, we argue that it is unlikely that the WTOW itself carries high-quality sPOM (see also Schulz et al., 2020), but the WTOW pycnocline can play a role in causing turbulence and water column mixing above the coral mound (Vic et al., 2019). Internal waves that propagate along this pycnocline can cause increased horizontal currents and vertical displacements (White et al., 2007; Pomar et al., 2012). Large variability in variables as temperature, density, and nutrient concentrations are therefore also seen as a proxy for internal wave activity (Davison et al., 2019).

Our measurements showed that the bottom water at Oreo was highly dynamic over the tidal cycle (Fig. 8, process 3a), *i.e.,* density, salinity, and buoyancy frequency there showed the highest variability close to the seafloor (supplements Fig. S12). This suggests that the water column above the mound is partly stratified and partly well-mixed during a 24-h tidal cycle, which could be the result of breaking internal waves on or over the steep topography. Similarly, intensified diurnal tidal waves have been observed close to the seafloor at Haas mound, a large CWC mound ±5 km to the north-east of Oreo mound (van Haren et al., 2014; Schulz et al., 2020). In addition, variability in nutrient concentrations was high in the bottom water at Oreo (e.g., range in NO_3^-: 12–18 μM), which was also found previously at other CWC reefs on Rockall Bank and Norway (McGrath et al., 2012; Findlay et al., 2015; Juva et al., 2021). Therefore, our data confirm that the water column at Oreo mound is more dynamic than at the top of Rockall bank (e.g., Mienis et al., 2007, 2009, 2012; Findlay et al., 2015), likely due to vertical water displacements by internal (tidal) waves. These vertical displacements would benefit the CWCs and associated community in two ways (Findlay et al., 2015): First, flushing of CWC reef bottom water with nutrient-rich colder water prevents build-up of low oxygen and nutrient conditions close to the CWC reef. Second, downward transport of warmer water containing fresh sPOM supplies high quality food to the CWC reef and thereby prevents bottom water depletion of high quality sPOM by the reef community (Lavaleye et al., 2009; Wagner et al., 2011).

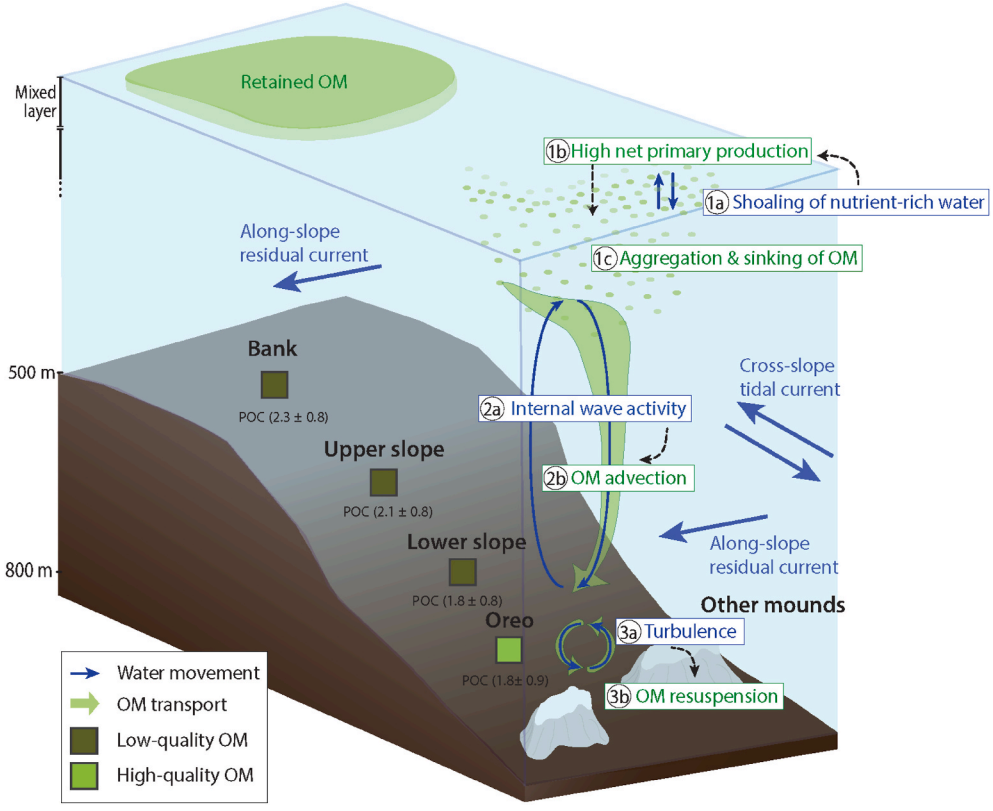

Fig. 8. Schematic illustration of the investigated transect. This illustration is not to scale and only indicates the organic matter-related transport processes argued in the current study. Hydrodynamic processes are indicated with blue arrows. Organic matter-related transport processes are indicated in green. OM = organic matter, POC = particulate organic matter concentration, in mean ± SD. Turbulence is here interpreted as a more dynamic bottom water layer over a tidal cycle. Along slope and cross slope transport arrows is based on Cyr et al. (2016) and Schulz et al. (2020).

4.2. Phytoplankton community dominated by diatoms

Primary productivity was higher in the surface waters at Bank and Upper slope compared to the Lower slope and Oreo, as indicated by higher concentrations of POC, chl-*a*, and CTD fluorescence. This is consistent with satellite data for chl-*a*, which shows that organic matter is retained on Rockall bank, while chl-*a* concentration decreases in surface waters in southward cross-slope direction (Mohn and White, 2007). The surface waters in the study area were dominated by diatoms, as shown by the dominance of fucoxanthin (Wright and Jeffrey, 1987; Barlow et al., 1993; Renaud et al., 2008) and the high EPA/DHA ratio in the *in-situ* pump samples, which compares well with previous work (Mojica et al., 2015). The chl-*a*:∑phaeopigment ratio of samples in the euphotic zone could be used to determine the growth phase of a phytoplankton community, where a ratio of >10 is indicative of growing healthy algae cells, and a ratio of 1:1 represents degraded material (Bianchi et al., 2002; Lomas and Moran, 2011). Furthermore, a high chlorophyllide-a concentration is indicative of senescent diatom cells (Bianchi et al., 2002; Jeffrey et al., 2005). Our results suggest that the diatom communities at the Bank and Upper slope were in a senescent phase (chl-*a*:∑phaeopigment ratio: 1.3 and 0.7 respectively; increasing chlorophyllide-a concentrations), while actively growing at Lower slope and Oreo (chl-*a*:∑phaeopigment ratio: 2.6 and 3.98 respectively; supplements Fig. S28). However, caution should be applied as high zooplankton grazing could also lower chl-*a*:∑phaeopigment ratio of surface water samples, and with the higher zooplankton biomass at Bank and Upper slope, this would suggest higher grazing activity at these sites (Louda et al., 2002).

Our findings also suggest that silicate is a limiting nutrient for phytoplankton growth in the euphotic zone. The near-1:1 correlation between surface nitrate and silicate concentrations (supplements Fig. S14) suggests that nitrate is taken up almost solely by diatoms (Brzezinski, 1985), implying that diatoms are largely responsible for new primary production in the euphotic zone, and that other phytoplankton species utilise regenerated nitrogen in the surface waters (Dugdale and Goering, 1967; Dugdale and Wilkerson, 1998). At the end of the 24-h cycle at Bank and Upper slope, surface water silicate concentrations became depleted, but the POC concentration and cryptophyte abundance still increased, suggesting regenerated production, and minimal diatom growth (Sonnekus et al., 2017).

The station Oreo exhibits shoaling of nutrient-rich water in the top 100 m surface layer during the tidal cycle (Fig. 8, process 1a; Fig. 5A; supplements Fig. S13), which could be the result of the diurnal tidal semi-enclosed Kelvin wave. The tidal wave likely supplies silicate to the surface layer and stimulates new primary production (Fig. 8, process 1b; Dugdale and Wilkerson, 1998). If this diurnal tidal wave reoccurs and replenishes nutrients in the surface layer at each tidal cycle along the slope of Rockall Bank, then new primary production could be elevated along the slope of Rockall Bank, and thus could be advected into the coral mound area from an upstream region (White et al., 2005; Soetaert et al., 2016). New primary production is equal to export production at steady state (i.e. Middelburg, 2019). As the sinking of ungrazed, large diatom cells and the formation of diatom aggregates are considered key mechanisms in export of POC to the deep sea (Boyd and Newton, 1999), these aggregates could enhance carbon export towards the coral mound (Fig. 8, process 1c). Previous research in the study area found that SPM in intermediate and bottom waters consisted mainly of biogenic material, such as diatoms and coccoliths, indicating this organic matter transport route can be important in the area (Mienis et al., 2007).

4.3. Increased organic matter quality at the coral mound and organic matter transport pathways

Food quantity and quality are drivers of benthic communities and food webs (Pearson and Rosenberg, 1978; Campanyà-Llovet et al., 2017). We report increased bottom water sPOM quality at the Oreo mound compared to the Bank site on a variety of temporal scales (12- and 24-h) and variables (C/N ratio, chl-*a*/phaeopigments, PUFA/-MUFA). The difference in sPOM quality between the stations along the transect is substantial, with a bottom-water chl-*a*:∑ phaeopigments ratio at Bank (0.57 ± 0.35) comparable with degraded sPOM from the Porcupine Abyssal Plain (North East Atlantic) at 4000 m depth, while at Oreo, the respective ratio (1.42 ± 1.06) is indicative of fresh/high quality material (Witbaard et al., 2000). The low quality sPOM at the Bank might be the result of organic matter retention on top of Rockall Bank, due to anticyclonic circulation of surface water around the bank summit (Mohn and White, 2007). The high variability of C/N ratios and $\delta^{13}C$ at Oreo, collected using Niskin bottles within the tidal cycle, indicates that the material originated from different sources, i.e., resuspended versus fresh sPOM (Fig. 8, processes 2b & 3b; supplements Fig. S24).

The higher organic matter quality at Oreo compared to the other stations is remarkable since the station is deeper than stations Bank and Upper slope. Nevertheless, high quality organic material can reach the seafloor through various pathways (Iversen and Lampitt, 2020), which are here demonstrated in a schematic illustration (Fig. 8): (i) Via advective downward transport of water from shallower depth which is especially important for small particles such as picoplankton (Fig. 8 process 2b; Richardson, 2019). (ii) High quality organic matter can also be transported towards the coral mound by lateral advection of resuspended, recently deposited fresh organic matter (Mienis et al., 2007). (iii) Organic matter can be transported downward cross-slope from the top of Rockall Bank to deep waters by 'Ekman drainage' (Simpson and McCandliss, 2013). (iv) Via formation and sinking of aggregates (Fig. 8, process 1c; Thiem et al., 2006). (v) Finally, zooplankton can also transport carbon to the seafloor by diel vertical migration (DVM; Steinberg, 1995).

Here, we observed a spike in organic matter quality and quantity of bottom-water sPOM, shortly after an internal wave passed the CWC mound (Fig. 5). Previous studies suggest a connection between internal tidal waves and organic matter freshness in the water column at CWC reefs (White et al., 2005; Mienis et al., 2007; Davies et al., 2009; Findlay et al., 2013; Soetaert et al., 2016), and link fluorescence with cross-slope tidal currents (Duineveld et al., 2007). High quality sPOM in bottom waters has been observed at several CWC mounds and reefs in the NE Atlantic (Kiriakoulakis et al., 2007). Furthermore, tidal downward transport of fresh sPOM to the seafloor has been recorded previously for shallow CWC reefs (~100–200 m depth) as Mingulay Reef (Davies et al., 2009; Duineveld et al., 2012) and Tisler Reef (Lavaleye et al., 2009). This study, when particularly looking at the nutrient data (Fig. 5, Fig. S13), provides evidence that water from shallower depth (~300 m), characterized by low density, low nutrient concentration, high sPOM quality, and increased picoplankton concentration, is advected downward to the CWC mound after the passing of a 200-m amplitude internal wave (Fig. 8, processes 2a & 2b). To our knowledge, this is the first study to report this for a relatively deep (750 m) CWC reef. A steady tidal supply of high-quality food particles is thought to be a key factor for healthy CWC reefs (Juva et al., 2020). Although there is currently no quantitative assessment of the state of the CWC reef on Oreo mound available, the images from an exploratory ROV dive and box core deployment videos suggest the presence of a flourishing CWC reef (Fig. 1 F; de Froe et al., 2019). The presence of a healthy reef suggests downward advection of high-quality organic matter occurs more frequently throughout the year.

In this study, we found no evidence for strong resuspension and consecutive 'Ekman drainage' across the SE slope of Rockall Bank. Although the *in-situ* pump data showed enhanced POC quantity at the Bank seafloor, which is consistent with the turbid bottom mixed layer observed during time of sampling3F,[4] no prominent benthic nepheloid

[4] Cruise report: 10.5281/zenodo.1454464.

layer was present cross-slope the Rockall Bank during both sampling campaigns (as in Thorpe and White, 1988; Simpson and McCandliss, 2013). This turbid layer on the Bank contained a relative high concentration of PUFAs in the large-fraction (>53 μm), which suggests bottom POC included large diatom-rich sPOM which had settled on the seafloor recently (Zimmerman and Canuel, 2001). Our CTD data did record slightly elevated turbidity in the bottom 200–300 m across the slope or Rockall Bank (turbid layer in Fig. 8, Figure S11 I-K). This could be the result of resuspension events caused by interaction of bottom current with other coral mounds located on the SE slope of Rockall Bank and would enhance organic matter transport across the slope towards the coral mound. However, although our data only provides a snapshot (24 h) in time, values are generally low and therefore large particulate matter transport seem unlikely. Furthermore, the slightly higher turbidity concentration at Oreo mound could also be advected by WTOW (Vlasenko and Stashchuk, 2018; Schulz et al., 2020).

The formation of diatom aggregates and their fast sinking through the water column relative to individual plankton (and their waste products) enhances transport of fresh organic material to the seafloor (Thiem et al., 2006; Iversen and Ploug, 2010). Support for this organic matter transport route at Oreo mound is found in the high EPA/DHA ratio in large sPOM in bottom waters, indicating the presence of diatoms. Accordingly, the lower $\delta^{15}N$ values of large sPOM compared to small sPOM at depth suggest that the large particles were fresher and hence transported faster to the bottom water. Additionally, micro- and mesozooplankton consume sPOM, thereby producing faecal pellets which, like aggregates, sink faster to the seafloor than smaller-sized sPOM (Youngbluth et al., 1989; Turner, 2015). The high concentration of zooplankton lipid biomarkers in bottom water sPOM (Fig. 7B), particularly in the small fraction (15–25 mol% of total lipids), indicate the presence of these pellets, and imply that the zooplankton generate small sized sPOM by mechanically breaking up larger sPOM/diatom aggregates. Alternatively, as zooplankton may store large amount of energy as lipids (Lee et al., 2006), the higher zooplankton lipid biomarker concentration in small sPOM could also be a result of high lipid content in bottom water zooplankton, which is supported by their high C/N ratio (supplements Fig. S26E). Finally, DVM was seen at Upper slope, with higher zooplankton biomass at the surface during the night and below 100 m depth during the day, but we could not verify the occurrence of DVM at Oreo due to sampling restrictions due to heavy weather. However, it is highly likely DVM took place at Oreo since the dominant zooplankton (calanoid copepods) are well known to migrate vertically (e.g. Zaret and Suffern, 1976; Bandara et al., 2021).

4.4. Organic matter composition and plankton densities over depth

In the bottom water, POC largely consists of detrital material, while phytoplankton-C stock contributes less than 10% (Fuhrman et al., 1989; Caron et al., 1995; Roman et al., 1995). However, caution should be applied in interpreting this estimation since the chl-*a*:POC ratio (1:40, de Jonge, 1980) can show high variability depending on the season, phytoplankton community, and nutrient availability (de Jonge, 1980; Murray et al., 1994; Taylor et al., 1997; Sathyendranath et al., 2009; Mojica et al., 2015). Although bacteria comprised the largest living fraction of POC in bottom waters, which was also found by Roman et al. (1995), phytoplankton was occasionally the largest fraction, for example, in the high organic matter quality sample from Oreo mound. This high phytoplankton fraction of POC measured at Oreo (compared to the Bank, Upper slope, and Lower slope) indicate transport of fresh organic matter to depth.

The high plankton density (nano-, pico-, bacterioplankton, and virus particles) in the bottom water above Oreo Mound compared to the other stations on the slope demonstrates an increased availability of fresh planktonic food. The bacterial density in the bottom water at Oreo ($1.6 \pm 0.8 \cdot 10^5$ cells mL^{-1}) was on average slightly lower than prokaryotic abundance in the bottom-water at a shallow CWC reef in the Skagerrak ($3.2 \pm 0.1 \cdot 10^5$ cells mL^{-1};Weinbauer et al., 2012) and at other deep coral mounds close to our transect (range $3.1–4.9 \cdot 10^5$ cells mL^{-1}; Maier et al., 2011; van Duyl et al., 2008). Viral particle density at Oreo ($2.8 \pm 1.1 \cdot 10^6$ cells mL^{-1}) was lower than that measured at Skagerrak ($1.1 \pm 0.1 \cdot 10^7$ mL^{-1}; Weinbauer et al., 2012) and at other coral mounds in the study area ($5.7–8.4 \cdot 10^6$ mL^{-1}; Maier et al., 2011). In the present study, the variability in cell/particle density was larger than at the Skagerrak reef and in earlier Rockall Bank measurements (van Duyl et al., 2008; Maier et al., 2011; Weinbauer et al., 2012). As zooplankton mostly feed on phytoplankton (Mauchline, 1998), their spatial distribution at the surface was closely linked to the chl-*a* concentration, with higher zooplankton biomass at Bank than at Oreo. We found decreasing zooplankton biomass with depth, consistent with observations on other North Atlantic zooplankton communities during spring (Gislason, 2018; Krumhansl et al., 2018). Overall, these findings show that, next to high variability in physical conditions (Juva et al., 2021) and higher sPOM quality, the plankton densities are increased close the CWC reef, indicating more food is available for suspension feeders living on the reef. Additionally, plankton densities were also highly variable over a single diurnal tidal cycle, a factor to consider in future sampling campaigns.

4.5. Food sources for the benthic communities

Our isotope and fatty acid data show that CWCs feed on a mixture of fresh phytodetritus, detritus, and smaller zooplankton, in agreement with previous work (Duineveld et al., 2007; van Oevelen et al., 2009; Galand et al., 2020). The $\delta^{15}N$ value of CWCs is comparable with previous observations at Rockall bank (8–8.5‰; Duineveld et al., 2007; Kiriakoulakis et al., 2005) and in the Mediterranean (Carlier et al., 2009), but lower compared to CWCs at Galicia bank (~9.5‰; Duineveld et al., 2004) and in Norwegian fjords (~10–11‰; Maier et al., 2020a). In the food web, CWCs are situated more than one trophic level above sPOM (assuming a 3.4‰ $\delta^{15}N$ enrichment per trophic level; Fry, 2006), indicating a mixed diet of sPOM and organisms of a higher trophic level, such as zooplankton (Mortensen, 2001). With respect to our third research objective, we could not, unfortunately, determine how important zooplankton is for the diet of CWCs. The stable isotopic signal of CWCs and presence of zooplankton-FATM imply CWCs might feed on zooplankton. Nevertheless, the observed presence of zooplankton-FATM in the CWC PLFAs alone is not enough to indicate a zooplankton diet, since CWCs can synthesize zooplankton-FATMs de novo (Mueller et al., 2014). Furthermore, at Rockall Bank, opposed to other CWC areas, zooplankton biomass in bottom waters in spring is low (present study, Duineveld et al., 2007). Nevertheless, the high food quality of lipid rich zooplankton (Lee et al., 2006), could imply CWCs only have to feed low amount of zooplankton to alter their trophic level. Alternatively, while CWC samples represent a longer time-integrated signal, the stable isotopic signal of sPOM and zooplankton biomass may vary on seasonal or annual scale. sPOM from sediment traps deployed at Oreo showed a higher $\delta^{15}N$ value in winter (~8‰) compared to spring (Korte et al., *in prep*), and more zooplankton were likely present in the bottom waters during winter and early spring when zooplankton (e.g. *Calanus* spp) are known to overwinter at depth (Heath et al., 2004). Therefore, the high trophic level of CWCs could originate from consumption of more degraded sPOM or higher zooplankton consumption in winter, as CWCs may switch their diet with seasonally changing food availability (Maier et al., 2020a). Nevertheless, a diet of mostly zooplankton appears unlikely. In addition, the corals may consume resuspended organic matter, as the sedimentary $\delta^{15}N$ (~5‰ was precisely one trophic level lower than the CWC samples. In comparison with CWCs, zooplankton could still be of importance for the CWC reef community, as the polychaete *E. norvegica*, which lives in symbiosis with *D. pertusum* and builds tubes within the coral framework (Mueller et al., 2013), showed relatively high concentration of zooplankton FATM and the $\delta^{15}N$ value (11–12‰) was one trophic level higher than large zooplankton (8‰). This compares well with literature (Duineveld et al., 2007; Mueller et al., 2013;

van Oevelen et al., 2018) and the observation that the polychaete can feed on suspended particles with their body extended up to 30 cm from the coral framework and steal food particles/zooplankton from polyps (Mortensen, 2001).

A further possible food source for the reef community is (labile) DOC, that can be taken up by a variety of deep-sea invertebrates (Rix et al., 2016; Maier et al., 2020b). We found elevated DOC concentrations in the bottom water (116 ± 73 μM) above Oreo as compared to the Bank (93 ± 23 μM). This higher DOC concentration at Oreo could originate from the sediment (Papadimitriou et al., 2002) and/or from reef biota such as CWCs (Wild et al., 2008; Maier et al., 2019). Other studies have also reported enhanced DOC concentrations above CWC reefs in the same study area (van Duyl et al., 2008; de Froe, unpublished data) and in the Skagerrak (Weinbauer et al., 2012) compared to open-ocean concentrations, indicating that CWC reefs are a source of DOC in the deep-sea (Wagner et al., 2011).

5. Conclusion

In summary, we have shown that the water column is more dynamic above a CWC mound at Rockall Bank in multiple ways. Our results suggest the presence of three organic matter transport mechanisms towards the coral mound. (1) Fresh organic matter of high quality is transported from mid-water depth to the seafloor by advection with internal waves (process 2a & 2b, Fig. 8). (2) Furthermore, the replenishment of surface nutrients may enhance new primary production of diatoms, which aggregate and sink to mid-water depth and ultimately the seafloor (process 1b & 1c, Fig. 8). (3) Lastly, zooplankton faecal pellets (and likely migration) may also enhance vertical transport of organic matter. The relative contribution of either of these mechanisms in fuelling the cold-water coral reef community remains to be clarified. Our study confirms that the reef benthic community feeds on a variety of food sources, yet ultimately depends on surface primary production.

Funding & author statement

This research was supported by the European Union's Horizon 2020 Research and Innovation Programme under grant agreement no. 678760 (ATLAS). This output reflects only the author's view, and the European Union cannot be held responsible for any use that may be made of the information contained therein. DvO and SM were supported by the Innovational Research Incentives Scheme of the Netherlands Organisation for Scientific Research (NWO), respectively, under grant agreement 864.13.007. We acknowledge the funding of the Netherlands Organisation for Scientific Research NWO and Royal Netherlands Institute for Sea Research NIOZ in organising the Netherlands Initiative Changing Oceans NICO expedition in 2018. The funders had no role in study design, data collection, and analysis, decision to publish, or preparation of the manuscript.

Declaration of competing interest

The authors declare that they have no known competing financial interests or personal relationships that could have appeared to influence the work reported in this paper.

Data availability

Data presented in this paper are provided at 10.5281/zenodo.6997532.

Acknowledgements

We would like to thank the skilful crew and technicians on board the R/V Pelagia for their support during the fieldwork. We would also like to thank Jan Peene, Peter van Breugel, Jurian Brasser, Yvonne van der Maas, Anna Noordeloos, and Kirsten Kooijman for their help in analysing all the samples. Further, we like to thank Pieter van Rijswijk for his help during fieldwork and in the laboratory. Finally, we want to thank Furu Mienis, Gerard Duineveld, and two anonymous reviewers for their constructive comments.

Appendix A. Supplementary data

Supplementary data to this article can be found online at https://doi.org/10.1016/j.dsr.2022.103854.

References

Addamo, A.M., Vertino, A., Stolarski, J., García-Jiménez, R., Taviani, M., Machordom, A., 2016. Merging scleractinian genera: the overwhelming genetic similarity between solitary *Desmophyllum* and colonial *Lophelia*. BMC Evol. Biol. 16, 108. https://doi.org/10.1186/s12862-016-0654-8.

Akima, H., Gebhardt, A., 2020. Akima: interpolation of irregularly and regularly spaced data. Available at: https://CRAN.R-project.org/package=akima.

Allaire, J.J., Xie, Y., McPherson, J., Luraschi, J., Ushey, K., Atkins, A., et al., 2021. Rmarkdown: dynamic documents for R. Available at: https://github.com/rstudio/rmarkdown.

Altabet, M.A., 1990. Organic C, N, and stable isotopic composition of particulate matter collected on glass-fiber and aluminum oxide filters. Limnol. Oceanogr. 35, 902–909. https://doi.org/10.4319/lo.1990.35.4.0902.

Bandara, K., Varpe, Ø., Wijewardene, L., Tverberg, V., Eiane, K., 2021. Two hundred years of zooplankton vertical migration research. Biol. Rev. 96, 1547–1589. https://doi.org/10.1111/brv.12715.

Barlow, R.G., Mantoura, R.F.C., Gough, M.A., Fileman, T.W., 1993. Pigment signatures of the phytoplankton composition in the northeastern Atlantic during the 1990 spring bloom. Deep Sea Res. Part II Top. Stud. Oceanogr. 40, 459–477. https://doi.org/10.1016/0967-0645(93)90027-K.

Bart, M.C., de Kluijver, A., Hoetjes, S., Absalah, S., Mueller, B., Kenchington, E., et al., 2020. Differential processing of dissolved and particulate organic matter by deep-sea sponges and their microbial symbionts. Sci. Rep. 10, 17515 https://doi.org/10.1038/s41598-020-74670-0.

Berggreen, U., Hansen, B., Kiørboe, T., 1988. Food size spectra, ingestion and growth of the copepod *Acartia tonsa* during development: implications for determination of copepod production. Mar. Biol. 99, 341–352. https://doi.org/10.1007/BF02112126.

Bianchi, T.S., Rolff, C., Widbom, B., Elmgren, R., 2002. Phytoplankton pigments in Baltic sea seston and sediments: seasonal variability, fluxes, and transformations. Estuar. Coast Shelf Sci. 55, 369–383. https://doi.org/10.1006/ecss.2001.0911.

Boschker, H.T.S., Brouwer, J. F. C. de, Cappenberg, T.E., 1999. The contribution of macrophyte-derived organic matter to microbial biomass in salt-marsh sediments: stable carbon isotope analysis of microbial biomarkers. Limnol. Oceanogr. 44, 309–319. https://doi.org/10.4319/lo.1999.44.2.0309.

Bourgault, D., Morsilli, M., Richards, C., Neumeier, U., Kelley, D.E., 2014. Sediment resuspension and nepheloid layers induced by long internal solitary waves shoaling orthogonally on uniform slopes. Continent. Shelf Res. 72, 21–33. https://doi.org/10.1016/j.csr.2013.10.019.

Boyd, P.W., Newton, P.P., 1999. Does planktonic community structure determine downward particulate organic carbon flux in different oceanic provinces? Deep-Sea Res. Part A Oceanogr. Res. Pap. 46, 63–91. https://doi.org/10.1016/S0967-0637(98)00066-1.

Brussaard, C.P.D., 2004. Optimization of procedures for counting viruses by flow cytometry. Appl. Environ. Microbiol. 70, 1506–1513. https://doi.org/10.1128/AEM.70.3.1506-1513.2004.

Brussaard, C.P.D., Noordeloos, A.A.M., Witte, H., Collenteur, M.C.J., Schulz, K., Ludwig, A., et al., 2013. Arctic microbial community dynamics influenced by elevated CO2 levels. Biogeosciences 10, 719–731. https://doi.org/10.5194/bg-10-719-2013.

Brzezinski, M.A., 1985. The Si:C:N ratio of marine diatoms: interspecific variability and the effect of some environmental variables. J. Phycol. 21, 347–357. https://doi.org/10.1111/j.0022-3646.1985.00347.x.

Campanyà-Llovet, N., Snelgrove, P.V.R., Parrish, C.C., 2017. Rethinking the importance of food quality in marine benthic food webs. Prog. Oceanogr. 156, 240–251. https://doi.org/10.1016/j.pocean.2017.07.006.

Carlier, A., Le Guilloux, E., Olu, K., Sarrazin, J., Mastrototaro, F., Taviani, M., et al., 2009. Trophic relationships in a deep mediterranean cold-water coral bank (Santa Maria di Leuca, Ionian sea). Mar. Ecol. Prog. Ser. 397, 125–137. https://doi.org/10.3354/meps08361.

Caron, D.A., Dam, H.G., Kremer, P., Lessard, E.J., Madin, L.P., Malone, T.C., et al., 1995. The contribution of microorganisms to particulate carbon and nitrogen in surface waters of the Sargasso Sea near Bermuda. Deep-Sea Res. Part A Oceanogr. Res. Pap. 42, 943–972. https://doi.org/10.1016/0967-0637(95)00027-4.

Casey, J.R., Aucan, J.P., Goldberg, S.R., Lomas, M.W., 2013. Changes in partitioning of carbon amongst photosynthetic pico- and nano-plankton groups in the Sargasso Sea in response to changes in the North Atlantic Oscillation. Deep Sea Res. Part II Top. Stud. Oceanogr. 93, 58–70. https://doi.org/10.1016/j.dsr2.2013.02.002.

Cho, B.C., Azam, F., 1988. Major role of bacteria in biogeochemical fluxes in the ocean's interior. Nature 332, 441–443. https://doi.org/10.1038/332441a0.

Christie, W.W., 1982. A simple procedure for rapid transmethylation of glycerolipids and cholesteryl esters. J. Lipid Res. 23, 1072–1075. https://doi.org/10.1016/S0022-2275(20)38081-0.
Cyr, F., Haren, H., Mienis, F., Duineveld, G., Bourgault, D., 2016. On the influence of cold-water coral mound size on flow hydrodynamics, and vice versa. Geophys. Res. Lett. 43, 775–783. https://doi.org/10.1002/2015GL067038.
Dalsgaard, J., St John, M., Kattner, G., Müller-Navarra, D., Hagen, W., 2003. Fatty acid trophic markers in the pelagic marine environment. In: Advances in Marine Biology. Elsevier, pp. 225–340. https://doi.org/10.1016/S0065-2881(03)46005-7.
Davies, A.J., Duineveld, G.C.A., Lavaleye, M.S.S., Bergman, M.J.N., van Haren, H., Roberts, J.M., 2009. Downwelling and deep-water bottom currents as food supply mechanisms to the cold-water coral *Lophelia pertusa* (Scleractinia) at the Mingulay Reef Complex. Limnol. Oceanogr. 54, 620–629. https://doi.org/10.4319/lo.2009.54.2.0620.
Davison, J.J., van Haren, H., Hosegood, P., Piechaud, N., Howell, K.L., 2019. The distribution of deep-sea sponge aggregations (Porifera) in relation to oceanographic processes in the Faroe-Shetland Channel. Deep-Sea Res. Part A Oceanogr. Res. Pap. 146, 55–61. https://doi.org/10.1016/j.dsr.2019.03.005.
De Clippele, L.H., Huvenne, V.A.I., Molodtsova, T.N., Roberts, J.M., 2019. The diversity and ecological role of non-scleractinian corals (Antipatharia and Alcyonacea) on scleractinian cold-water coral mounds. Front. Mar. Sci. 6, 184. https://doi.org/10.3389/fmars.2019.00184.
de Froe, E., Rovelli, L., Glud, R.N., Maier, S.R., Duineveld, G., Mienis, F., et al., 2019. Benthic oxygen and nitrogen exchange on a cold-water coral reef in the north-east Atlantic ocean. Front. Mar. Sci. 6, 665. https://doi.org/10.3389/fmars.2019.00665.
de Haas, H., Mienis, F., Frank, N., Richter, T.O., Steinacher, R., de Stigter, H., et al., 2009. Morphology and sedimentology of (clustered) cold-water coral mounds at the south Rockall Trough margins, NE Atlantic Ocean. Facies 55, 1–26. https://doi.org/10.1007/s10347-008-0157-1.
de Jonge, V., 1980. Fluctuations in the organic carbon to chlorophyll a ratios for estuarine benthic diatom populations. Mar. Ecol. Prog. Ser. 2, 345–353. https://doi.org/10.3354/meps002345.
Dugdale, R.C., Goering, J.J., 1967. Uptake of new and regenerated forms of nitrogen in primary productivity. Limnol. Oceanogr. 12, 196–206. https://doi.org/10.4319/lo.1967.12.2.0196.
Dugdale, R.C., Wilkerson, F.P., 1998. Silicate regulation of new production in the equatorial Pacific upwelling. Nature 391, 270–273. https://doi.org/10.1038/34630.
Duineveld, G.C.A., Lavaleye, M.S.S., Bergman, M.J.N., de Stigter, H., Mienis, F., 2007. Trophic structure of a cold-water coral mound community (Rockall Bank, NE Atlantic) in relation to the near-bottom particle supply and current regime. Bull. Mar. Sci. 81, 19.
Duineveld, G., Jeffreys, R., Lavaleye, M., Davies, A., Bergman, M., Watmough, T., et al., 2012. Spatial and tidal variation in food supply to shallow cold-water coral reefs of the Mingulay Reef complex (Outer Hebrides, Scotland). Mar. Ecol. Prog. Ser. 444, 97–115. https://doi.org/10.3354/meps09430.
Duineveld, G., Lavaleye, M., Berghuis, E., 2004. Particle flux and food supply to a seamount cold-water coral community (Galicia Bank, NW Spain). Mar. Ecol. Prog. Ser. 277, 13–23. https://doi.org/10.3354/meps277013.
Dullo, W.C., Flögel, S., Rüggeberg, A., 2008. Cold-water coral growth in relation to the hydrography of the Celtic and Nordic European continental margin. Mar. Ecol. Prog. Ser. 371, 165–176. https://doi.org/10.3354/meps07623.
Egbert, G.D., Erofeeva, S.Y., 2002. Efficient inverse modeling of barotropic ocean tides. J. Atmos. Ocean. Technol. 19, 183–204, 10.1175/1520-0426(2002)019<0183:EIMOBO>2.0.CO;2.
Fanelli, E., Cartes, J.E., Papiol, V., 2011a. Food web structure of deep-sea macrozooplankton and micronekton off the Catalan slope: insight from stable isotopes. J. Mar. Syst. 87, 79–89. https://doi.org/10.1016/j.jmarsys.2011.03.003.
Fanelli, E., Papiol, V., Cartes, J.E., Rumolo, P., Brunet, C., Sprovieri, M., 2011b. Food web structure of the epibenthic and infaunal invertebrates on the Catalan slope (NW Mediterranean): evidence from δ13C and δ15N analysis. Deep-Sea Res. Part A Oceanogr. Res. Pap. 58, 98–109. https://doi.org/10.1016/j.dsr.2010.12.005.
Findlay, H.S., Artioli, Y., Moreno Navas, J., Hennige, S.J., Wicks, L.C., Huvenne, V.A.I., et al., 2013. Tidal downwelling and implications for the carbon biogeochemistry of cold-water corals in relation to future ocean acidification and warming. Global Change Biol. 19, 2708–2719. https://doi.org/10.1111/gcb.12256.
Findlay, H.S., Hennige, S.J., Wicks, L.C., Navas, J.M., Woodward, E.M.S., Roberts, J.M., 2015. Fine-scale nutrient and carbonate system dynamics around cold-water coral reefs in the northeast Atlantic. Sci. Rep. 4, 3671. https://doi.org/10.1038/srep03671.
Fry, B., 2006. Stable Isotope Ecology. Springer-Verlag, New York. https://doi.org/10.1007/0-387-33745-8.
Fuhrman, J., Sleeter, T., Carlson, C., Proctor, L., 1989. Dominance of bacterial biomass in the Sargasso Sea and its ecological implications. Mar. Ecol. Prog. Ser. 57, 207–217. https://doi.org/10.3354/meps057207.
Galand, P.E., Remize, M., Meistertzheim, A., Pruski, A.M., Peru, E., Suhrhoff, T.J., et al., 2020. Diet shapes cold-water corals bacterial communities. Environ. Microbiol. 22, 354–368. https://doi.org/10.1111/1462-2920.14852.
Gerkema, T., 2019. An Introduction to Tides. Cambridge University Press, Cambridge. https://doi.org/10.1017/9781316998793.
Gislason, A., 2018. Life cycles and seasonal vertical distributions of copepods in the Iceland Sea. Polar Biol. 41, 2575–2589. https://doi.org/10.1007/s00300-018-2392-4.
Gori, A., Grover, R., Orejas, C., Sikorski, S., Ferrier-Pagès, C., 2014. Uptake of dissolved free amino acids by four cold-water coral species from the Mediterranean Sea. Deep Sea Res. Part II Top. Stud. Oceanogr. 99, 42–50. https://doi.org/10.1016/j.dsr2.2013.06.007.
Gori, A., Reynaud, S., Orejas, C., Ferrier-Pagès, C., 2015. The influence of flow velocity and temperature on zooplankton capture rates by the cold-water coral Dendrophyllia cornigera. J. Exp. Mar. Biol. Ecol. 466, 92–97. https://doi.org/10.1016/j.jembe.2015.02.004.
Grolemund, G., Wickham, H., 2011. Dates and times made easy with lubridate. J. Stat. Software 40, 1–25.
Hansen, B., Østerhus, S., 2000. North Atlantic–Nordic seas exchanges. Prog. Oceanogr. 45, 109–208. https://doi.org/10.1016/S0079-6611(99)00052-X.
Heath, M.R., Boyle, P.R., Gislason, A., Gurney, W.S.C., Hay, S.J., Head, E.J.H., et al., 2004. Comparative ecology of over-wintering Calanus finmarchicus in the northern North Atlantic, and implications for life-cycle patterns. ICES J. Mar. Sci. 61, 698–708. https://doi.org/10.1016/j.icesjms.2004.03.013.
Henry, L.-A., Roberts, J.M., 2007. Biodiversity and ecological composition of macrobenthos on cold-water coral mounds and adjacent off-mound habitat in the bathyal Porcupine Seabight, NE Atlantic. Deep-Sea Res. Part A Oceanogr. Res. Pap. 54, 654–672. https://doi.org/10.1016/j.dsr.2007.01.005.
Hirche, H.-J., Mumm, N., 1992. Distribution of dominant copepods in the Nansen basin, Arctic ocean, in summer. Deep-Sea Res. Part A Oceanogr. Res. Pap. 39, S485–S505. https://doi.org/10.1016/S0198-0149(06)80017-8.
Holliday, N.P., Pollard, R.T., Read, J.F., Leach, H., 2000. Water mass properties and fluxes in the Rockall Trough, 1975 - 1998. Deep-Sea Res. Part A Oceanogr. Res. Pap. 1303–1332.
Hosegood, P., van Haren, H., 2004. Near-bed solibores over the continental slope in the Faeroe-Shetland Channel. Deep Sea Res. Part II Top. Stud. Oceanogr. 51, 2943–2971. https://doi.org/10.1016/j.dsr2.2004.09.016.
Huthnance, J.M., 1973. On the diurnal tidal currents over Rockall Bank. Deep Sea Res. 21, 23–35.
Hygum, B.H., Rey, C., Hansen, B.W., 2000. Growth and development rates of *Calanus finmarchicus* nauplii during a diatom spring bloom. Mar. Biol. 136, 1075–1085. https://doi.org/10.1007/s002270000313.
Iken, K., Brey, T., Wand, U., Voigt, J., Junghans, P., 2001. Food web structure of the benthic community at the Porcupine Abyssal Plain (NE Atlantic): a stable isotope analysis. Prog. Oceanogr. 50, 383–405. https://doi.org/10.1016/S0079-6611(01)00062-3.
Iversen, M.H., Lampitt, R.S., 2020. Size does not matter after all: No evidence for a size-sinking relationship for marine snow. Prog. Oceanogr. 189, 102445 https://doi.org/10.1016/j.pocean.2020.102445.
Iversen, M.H., Ploug, H., 2010. Ballast minerals and the sinking carbon flux in the ocean: carbon-specific respiration rates and sinking velocity of marine snow aggregates. Biogeosciences 7, 2613–2624. https://doi.org/10.5194/bg-7-2613-2010.
Jeffrey, S.W., Mantoura, R.F.C., Wright, S.W., 2005. Phytoplankton Pigments in Oceanography: Guidelines to Modern Methods. Unesco Pub, Paris, France.
Johnson, C., Sherwin, T., Cunningham, S., Dumont, E., Houpert, L., Holliday, N.P., 2017. Transports and pathways of overflow water in the Rockall Trough. Deep-Sea Res. Part A Oceanogr. Res. Pap. 122, 48–59. https://doi.org/10.1016/j.dsr.2017.02.004.
Johnson, C., Sherwin, T., Smythe-Wright, D., Shimmield, T., Turrell, W., 2010. Wyville Thomson Ridge overflow water: spatial and temporal distribution in the Rockall trough. Deep-Sea Res. Part A Oceanogr. Res. Pap. 57, 1153–1162. https://doi.org/10.1016/j.dsr.2010.07.006.
Juva, K., Flögel, S., Karstensen, J., Linke, P., Dullo, W.-C., 2020. Tidal dynamics control on cold-water coral growth: a high-resolution multivariable study on eastern Atlantic cold-water coral sites. Front. Mar. Sci. 7, 132. https://doi.org/10.3389/fmars.2020.00132.
Juva, K., Kutti, T., Chierici, M., Dullo, W.-C., Flögel, S., 2021. Cold-water coral reefs in the Langenuen Fjord, Southwestern Norway—a window into future environmental change. Oceans 2, 583–610. https://doi.org/10.3390/oceans2030033.
Kelley, D., Richards, C., 2020. Oce: analysis of oceanographic data. Available at: https://CRAN.R-project.org/package=oce.
Kenyon, N.H., Akhmetzhanov, A.M., Wheeler, A.J., van Weering, T.C.E., de Haas, H., Ivanov, M.K., 2003. Giant carbonate mud mounds in the southern Rockall Trough. Mar. Geol. 195, 5–30. https://doi.org/10.1016/S0025-3227(02)00680-1.
Kiriakoulakis, K., Fisher, E., Wolff, G.A., Freiwald, A., Grehan, A., Roberts, J.M., 2005. Lipids and nitrogen isotopes of two deep-water corals from the North-East Atlantic: initial results and implications for their nutrition. In: Freiwald, A., Roberts, J.M. (Eds.), Cold-Water Corals and Ecosystems. Springer-Verlag, Berlin/Heidelberg, pp. 715–729. https://doi.org/10.1007/3-540-27673-4_37.
Kiriakoulakis, K., Freiwald, A., Fisher, E., Wolff, G.A., 2007. Organic matter quality and supply to deep-water coral/mound systems of the NW European Continental Margin. Int. J. Earth Sci. 96, 159–170. https://doi.org/10.1007/s00531-006-0078-6.
Klein Breteler, W.C.M., 1982. The life stages of four pelagic copepods (Copepoda: calanoida), illustrated by a series of photographs: Klein Breteler, W.C.M., 1982. (Acartia clausi, Temora longicornis, Centropages hamatus and Pseudocalanus sp.). Publ. Ser. Neth. Inst. Sea Res., 6:32pp. Deep Sea Res. Part B Oceanogr. Lit. Rev. 30, 934. https://doi.org/10.1016/0198-0254(83)96590-1.
Krumhansl, K.A., Head, E.J.H., Pepin, P., Plourde, S., Record, N.R., Runge, J.A., et al., 2018. Environmental drivers of vertical distribution in diapausing Calanus copepods in the Northwest Atlantic. Prog. Oceanogr. 162, 202–222. https://doi.org/10.1016/j.pocean.2018.02.018.
Lampitt, R.S., Wishner, K.F., Turley, C.M., Angel, M.V., 1993. Marine snow studies in the Northeast Atlantic Ocean: distribution, composition and role as a food source for migrating plankton. Mar. Biol. 116, 689–702. https://doi.org/10.1007/BF00355486.
Larsson, A.I., Lundälv, T., van Oevelen, D., 2013. Skeletal growth, respiration rate and fatty acid composition in the cold-water coral *Lophelia pertusa* under varying food conditions. Mar. Ecol. Prog. Ser. 483, 169–184. https://doi.org/10.3354/meps10284.

Lavaleye, M., Duineveld, G., Lundälv, T., White, M., Guihen, D., Kiriakoulakis, K., et al., 2009. Cold-water corals on the Tisler reef: preliminary observations on the dynamic reef environment. Oceanography 22, 76–84.
Lavaleye, M.S.S., Duineveld, G.C.A., Berghuis, E.M., Kok, A., Witbaard, R., 2002. A comparison between the megafauna communities on the N.W. Iberian and Celtic continental margins—effects of coastal upwelling? Prog. Oceanogr. 52, 459–476. https://doi.org/10.1016/S0079-6611(02)00019-8.
Lee, R.F., Hagen, W., Kattner, G., 2006. Lipid storage in marine zooplankton. Mar. Ecol. Prog. Ser. 307, 273–306. https://doi.org/10.3354/meps307273.
Lee, S., Fuhrman, J.A., 1987. Relationships between biovolume and biomass of naturally derived marine bacterioplankton. Appl. Environ. Microbiol. 53, 1298–1303.
Lomas, M.W., Moran, S.B., 2011. Evidence for aggregation and export of cyanobacteria and nano-eukaryotes from the Sargasso Sea euphotic zone. Biogeosciences 8, 203–2016. https://doi.org/10.5194/bg-8-203-2011.
Louda, J.W., Liu, L., Baker, E.W., 2002. Senescence- and death-related alteration of chlorophylls and carotenoids in marine phytoplankton. Org. Geochem. 33, 1635–1653. https://doi.org/10.1016/S0146-6380(02)00106-7.
Madsen, S.D., Nielsen, T.G., Hansen, B.W., 2001. Annual population development and production by Calanus finmarchicus , C. glacialis and C. hyperboreus in Disko Bay, western Greenland. Mar. Biol. 139, 75–93. https://doi.org/10.1007/s002270100552.
Maier, C., de Kluijver, A., Agis, M., Brussaard, C.P.D., van Duyl, F.C., Weinbauer, M.G., 2011. Dynamics of nutrients, total organic carbon, prokaryotes and viruses in onboard incubations of cold-water corals. Biogeosciences 8, 2609–2620. https://doi.org/10.5194/bg-8-2609-2011.
Maier, S.R., Bannister, R.J., van Oevelen, D., Kutti, T., 2020a. Seasonal controls on the diet, metabolic activity, tissue reserves and growth of the cold-water coral *Lophelia pertusa*. Coral Reefs 39, 173–187. https://doi.org/10.1007/s00338-019-01886-6.
Maier, S.R., Kutti, T., Bannister, R.J., Fang, J.K.-H., van Breugel, P., van Rijswijk, P., et al., 2020b. Recycling pathways in cold-water coral reefs: use of dissolved organic matter and bacteria by key suspension feeding taxa. Sci. Rep. 10, 9942. https://doi.org/10.1038/s41598-020-66463-2.
Maier, S.R., Kutti, T., Bannister, R.J., van Breugel, P., van Rijswijk, P., van Oevelen, D., 2019. Survival under conditions of variable food availability: resource utilization and storage in the cold-water coral *Lophelia pertusa*: cold-water coral resource utilization and storage. Limnol. Oceanogr. 64, 1651–1671. https://doi.org/10.1002/lno.11142.
Maier, S.R., Mienis, F., de Froe, E., Soetaert, K., Lavaleye, M., Duineveld, G., et al., 2021. Reef communities associated with 'dead' cold-water coral framework drive resource retention and recycling in the deep sea. Deep-Sea Res. Part A Oceanogr. Res. Pap. 175 https://doi.org/10.1016/j.dsr.2021.103574.
Marie, D., Partensky, F., Vaulot, D., Brussaard, C., 1999. Enumeration of phytoplankton, bacteria, and viruses in marine samples. Curr. Protoc. Cytom. 10, 11. https://doi.org/10.1002/0471142956.cy1111s10, 11.1-11.11.15.
Mauchline, J., 1998. The Biology of Calanoid Copepods. Academic Press, San Diego.
McGrath, T., Nolan, G., McGovern, E., 2012. Chemical characteristics of water masses in the Rockall Trough. Deep-Sea Res. Part A Oceanogr. Res. Pap. 61, 57–73. https://doi.org/10.1016/j.dsr.2011.11.007.
Michna, P., Woods, M., 2019. RNetCDF: Interface to "NetCDF" datasets. Available at: https://CRAN.R-project.org/package=RNetCDF.
Middelbo, A.B., Sejr, M.K., Arendt, K.E., Møller, E.F., 2018. Impact of glacial meltwater on spatiotemporal distribution of copepods and their grazing impact in Young Sound NE, Greenland. Limnol. Oceanogr. 63, 322–336. https://doi.org/10.1002/lno.10633.
Middelburg, J.J., 2019. Marine Carbon Biogeochemistry: A Primer for Earth System Scientists. Springer International Publishing, Cham, Switzerland. https://doi.org/10.1007/978-3-030-10822-9.
Mienis, F., de Stigter, H.C., de Haas, H., van Weering, T.C.E., 2009a. Near-bed particle deposition and resuspension in a cold-water coral mound area at the Southwest Rockall Trough margin, NE Atlantic. Deep-Sea Res. Part A Oceanogr. Res. Pap. 56, 1026–1038. https://doi.org/10.1016/j.dsr.2009.01.006.
Mienis, F., de Stigter, H.C., White, M., Duineveld, G., de Haas, H., van Weering, T.C.E., 2007. Hydrodynamic controls on cold-water coral growth and carbonate-mound development at the SW and SE Rockall Trough Margin, NE Atlantic Ocean. Deep-Sea Res. Part A Oceanogr. Res. Pap. 54, 1655–1674. https://doi.org/10.1016/j.dsr.2007.05.013.
Mienis, F., Duineveld, G.C.A., Davies, A.J., Ross, S.W., Seim, H., Bane, J., et al., 2012. The influence of near-bed hydrodynamic conditions on cold-water corals in the Viosca Knoll area, Gulf of Mexico. Deep-Sea Res. Part A Oceanogr. Res. Pap. 60, 32–45. https://doi.org/10.1016/j.dsr.2011.10.007.
Mienis, F., van der Land, C., de Stigter, H.C., van de Vorstenbosch, M., de Haas, H., Richter, T., et al., 2009b. Sediment accumulation on a cold-water carbonate mound at the Southwest Rockall Trough margin. Mar. Geol. 265, 40–50. https://doi.org/10.1016/j.margeo.2009.06.014.
Mienis, F., van Weering, T., de Haas, H., de Stigter, H., Huvenne, V., Wheeler, A., 2006. Carbonate mound development at the SW Rockall Trough margin based on high resolution TOBI and seismic recording. Mar. Geol. 233, 1–19. https://doi.org/10.1016/j.margeo.2006.08.003.
Mohn, C., Rengstorf, A., White, M., Duineveld, G., Mienis, F., Soetaert, K., et al., 2014. Linking benthic hydrodynamics and cold-water coral occurrences: a high-resolution model study at three cold-water coral provinces in the NE Atlantic. Prog. Oceanogr. 122, 92–104. https://doi.org/10.1016/j.pocean.2013.12.003.
Mohn, C., White, M., 2007. Remote sensing and modelling of bio-physical distribution patterns at porcupine and Rockall bank, Northeast Atlantic. Continent. Shelf Res. 27, 1875–1892. https://doi.org/10.1016/j.csr.2007.03.006.
Mojica, K.D.A., van de Poll, W.H., Kehoe, M., Huisman, J., Timmermans, K.R., Buma, A. G.J., et al., 2015. Phytoplankton community structure in relation to vertical stratification along a north-south gradient in the Northeast Atlantic Ocean: phytoplankton and vertical stratification. Limnol. Oceanogr. 60, 1498–1521. https://doi.org/10.1002/lno.10113.
Mortensen, P.B., 2001. Aquarium observations on the deep-water coral *Lophelia pertusa* (L., 1758) (scleractinia) and selected associated invertebrates. Ophelia 54, 83–104. https://doi.org/10.1080/00785236.2001.10409457.
Mueller, C.E., Larsson, A.I., Veuger, B., Middelburg, J.J., van Oevelen, D., 2014. Opportunistic feeding on various organic food sources by the cold-water coral *Lophelia pertusa*. Biogeosciences 11, 123–133. https://doi.org/10.5194/bg-11-123-2014.
Mueller, C.E., Lundälv, T., Middelburg, J.J., van Oevelen, D., 2013. The symbiosis between *Lophelia pertusa* and *Eunice norvegica* stimulates coral calcification and worm Assimilation. PLoS One 8, e58660. https://doi.org/10.1371/journal.pone.0058660.
Murray, J.W., Barber, R.T., Roman, M.R., Bacon, M.P., Feely, R.A., 1994. Physical and biological controls on carbon cycling in the equatorial pacific. Science 266, 58–65. https://doi.org/10.1126/science.266.5182.58.
Naumann, M.S., Orejas, C., Wild, C., Ferrier-Pages, C., 2011. First evidence for zooplankton feeding sustaining key physiological processes in a scleractinian cold-water coral. J. Exp. Biol. 214, 3570–3576. https://doi.org/10.1242/jeb.061390.
Neuwirth, E., 2014. RColorBrewer: ColorBrewer palettes. Available at: https://CRAN.R-project.org/package=RColorBrewer.
Ogle, D.H., Wheeler, P., Dinno, A., 2021. FSA: fisheries stock analysis. Available at: https://github.com/droglenc/FSA.
Papadimitriou, S., Kennedy, H., Bentaleb, I., Thomas, D.N., 2002. Dissolved organic carbon in sediments from the eastern North Atlantic. Mar. Chem. 79, 37–47. https://doi.org/10.1016/S0304-4203(02)00055-5.
Pearson, T., Rosenberg, R., 1978. Macrobenthic succession in relation to organic enrichment and pollution of the marine environment. In: Oceanography and Marine Biology—An Annual Review, pp. 229–311. https://doi.org/10.2983/035.034.0121U1.10.
Pomar, L., Morsilli, M., Hallock, P., Bádenas, B., 2012. Internal waves, an under-explored source of turbulence events in the sedimentary record. Earth Sci. Rev. 111, 56–81. https://doi.org/10.1016/j.earscirev.2011.12.005.
Purser, A., Larsson, A.I., Thomsen, L., van Oevelen, D., 2010. The influence of flow velocity and food concentration on *Lophelia pertusa* (Scleractinia) zooplankton capture rates. J. Exp. Mar. Biol. Ecol. 395, 55–62. https://doi.org/10.1016/j.jembe.2010.08.013.
R Core Team, 2019. R: a language and environment for statistical computing. Available at: https://www.R-project.org/.
Raddatz, J., Rüggeberg, A., Liebetrau, V., Foubert, A., Hathorne, E.C., Fietzke, J., et al., 2014. Environmental boundary conditions of cold-water coral mound growth over the last 3 million years in the Porcupine Seabight, Northeast Atlantic. Deep Sea Res. Part II Top. Stud. Oceanogr. 99, 227–236. https://doi.org/10.1016/j.dsr2.2013.06.009.
Renaud, P.E., Morata, N., Carroll, M.L., Denisenko, S.G., Reigstad, M., 2008. Pelagic–benthic coupling in the western Barents Sea: processes and time scales. Deep Sea Res. Part II Top. Stud. Oceanogr. 55, 2372–2380. https://doi.org/10.1016/j.dsr2.2008.05.017.
Ribeiro, C., Lopes dos Santos, A., Marie, D., Helena Pellizari, V., Pereira Brandini, F., Vaulot, D., 2016. Pico and nanoplankton abundance and carbon stocks along the Brazilian Bight. PeerJ 4, e2587. https://doi.org/10.7717/peerj.2587.
Richardson, T.L., 2019. Mechanisms and pathways of small-phytoplankton export from the surface ocean. Ann. Rev. Mar. Sci 11, 57–74. https://doi.org/10.1146/annurev-marine-121916-063627.
Rix, L., de Goeij, J.M., Mueller, C.E., Struck, U., Middelburg, J.J., van Duyl, F.C., et al., 2016. Coral mucus fuels the sponge loop in warm- and cold-water coral reef ecosystems. Sci. Rep. 6, 18715 https://doi.org/10.1038/srep18715.
Roberts, J., Davies, A., Henry, L., Dodds, L., Duineveld, G., Lavaleye, M., et al., 2009. Mingulay reef complex: an interdisciplinary study of cold-water coral habitat, hydrography and biodiversity. Mar. Ecol. Prog. Ser. 397, 139–151. https://doi.org/10.3354/meps08112.
Roberts, J.M., Wheeler, A.J., Freiwald, A., 2006. Reefs of the deep: the biology and geology of cold-water coral ecosystems. Science 312, 543–547. https://doi.org/10.1126/science.1119861.
Roman, M.R., Caron, D.A., Kremer, P., Lessard, E.J., Madin, L.P., Malone, T.C., et al., 1995. Spatial and temporal changes in the partitioning of organic carbon in the plankton community of the Sargasso Sea off Bermuda. Deep-Sea Res. Part A Oceanogr. Res. Pap. 42, 973–992. https://doi.org/10.1016/0967-0637(95)00028-5.
Rüggeberg, A., Flögel, S., Dullo, W.-C., Raddatz, J., Liebetrau, V., 2016. Paleoseawater density reconstruction and its implication for cold-water coral carbonate mounds in the northeast Atlantic through time: seawater density and carbonate mounds. Paleoceanography 31, 365–379. https://doi.org/10.1002/2015PA002859.
Sabatini, M., Kiørboe, T., 1994. Egg production, growth and development of the cyclopoid copepod Oithona similis. J. Plankton Res. 16, 1329–1351. https://doi.org/10.1093/plankt/16.10.1329.
Satapoomin, S., 1999. Carbon content of some common tropical Andaman Sea copepods. J. Plankton Res. 21, 2117–2123.
Sathyendranath, S., Stuart, V., Nair, A., Oka, K., Nakane, T., Bouman, H., et al., 2009. Carbon-to-chlorophyll ratio and growth rate of phytoplankton in the sea. Mar. Ecol. Prog. Ser. 383, 73–84. https://doi.org/10.3354/meps07998.
Schulz, K., Soetaert, K., Mohn, C., Korte, L., Mienis, F., Duineveld, G., et al., 2020. Linking large-scale circulation patterns to the distribution of cold water corals along

the eastern Rockall Bank (northeast Atlantic). J. Mar. Syst. 212, 103456 https://doi.org/10.1016/j.jmarsys.2020.103456.
Simpson, J.H., McCandliss, R.R., 2013. The Ekman Drain": a conduit to the deep ocean for shelf material. Ocean Dynam. 63, 1063–1072. https://doi.org/10.1007/s10236-013-0644-y.
Soetaert, K., 2019a. OceanView: visualisation of oceanographic data and model output. Available at: https://CRAN.R-project.org/package=OceanView.
Soetaert, K., 2019b. plot3D: plotting multi-dimensional data. Available at: https://CRAN.R-project.org/package=plot3D.
Soetaert, K., Mohn, C., Rengstorf, A., Grehan, A., van Oevelen, D., 2016. Ecosystem engineering creates a direct nutritional link between 600-m deep cold-water coral mounds and surface productivity. Sci. Rep. 6, 35057 https://doi.org/10.1038/srep35057.
Sonnekus, M.J., Bornman, T.G., Campbell, E.E., 2017. Phytoplankton and nutrient dynamics of six South West Indian Ocean seamounts. Deep-Sea Res. Part II Top. Stud. Oceanogr. 136, 59–72. https://doi.org/10.1016/j.dsr2.2016.12.008.
Steinberg, D.K., 1995. Diet of copepods (Scopalatum vorax) associated with mesopelagic detritus (giant larvacean houses) in Monterey Bay, California. Mar. Biol. 122, 571–584. https://doi.org/10.1007/BF00350679.
Suttle, C.A., 2005. Viruses in the sea. Nature 437, 356–361. https://doi.org/10.1038/nature04160.
Tarran, G.A., Heywood, J.L., Zubkov, M.V., 2006. Latitudinal changes in the standing stocks of nano- and picoeukaryotic phytoplankton in the Atlantic Ocean. Deep Sea Res. Part II Top. Stud. Oceanogr. 53, 1516–1529.
Taylor, A., Geider, R., Gilbert, F., 1997. Seasonal and latitudinal dependencies of phytoplankton carbon-to-chlorophyll a ratios:results of a modelling study. Mar. Ecol. Prog. Ser. 152, 51–66. https://doi.org/10.3354/meps152051.
Thiem, Ø., Ravagnan, E., Fosså, J.H., Berntsen, J., 2006. Food supply mechanisms for cold-water corals along a continental shelf edge. J. Mar. Syst. 60, 207–219. https://doi.org/10.1016/j.jmarsys.2005.12.004.
Thorpe, S.A., White, M., 1988. A deep intermediate nepheloid layer. Deep-Sea Res. Part A Oceanogr. Res. Pap. 35, 1665–1671. https://doi.org/10.1016/0198-0149(88)90109-4.
Turner, J.T., 2015. Zooplankton fecal pellets, marine snow, phytodetritus and the ocean's biological pump. Prog. Oceanogr. 130, 205–248. https://doi.org/10.1016/j.pocean.2014.08.005.
van der Kaaden, A.-S., Mohn, C., Gerkema, T., Maier, S.R., de Froe, E., van de Koppel, J., et al., 2021. Feedbacks between hydrodynamics and cold-water coral mound development. Deep-Sea Res. Part A Oceanogr. Res. Pap. 178, 103641 https://doi.org/10.1016/j.dsr.2021.103641.
van Duyl, F., Hegeman, J., Hoogstraten, A., Maier, C., 2008. Dissolved carbon fixation by sponge–microbe consortia of deep water coral mounds in the northeastern Atlantic Ocean. Mar. Ecol. Prog. Ser. 358, 137–150. https://doi.org/10.3354/meps07370.
Van Engeland, T., Godø, O.R., Johnsen, E., Duineveld, G.C.A., van Oevelen, D., 2019. Cabled ocean observatory data reveal food supply mechanisms to a cold-water coral reef. Prog. Oceanogr. 172, 51–64. https://doi.org/10.1016/j.pocean.2019.01.007.
van Haren, H., Mienis, F., Duineveld, G.C.A., Lavaleye, M.S.S., 2014. High-resolution temperature observations of a trapped nonlinear diurnal tide influencing cold-water corals on the Logachev mounds. Prog. Oceanogr. 125, 16–25. https://doi.org/10.1016/j.pocean.2014.04.021.
van Oevelen, D., Duineveld, G.C.A., Lavaleye, M.S.S., Kutti, T., Soetaert, K., 2018. Trophic structure of cold-water coral communities revealed from the analysis of tissue isotopes and fatty acid composition. Mar. Biol. Res. 14, 287–306. https://doi.org/10.1080/17451000.2017.1398404.
van Oevelen, D., Duineveld, G., Lavaleye, M., Mienis, F., Soetaert, K., Heip, C.H.R., 2009. The cold-water coral community as hotspot of carbon cycling on continental margins: a food-web analysis from Rockall Bank (northeast Atlantic). Limnol. Oceanogr. 54, 1829–1844. https://doi.org/10.4319/lo.2009.54.6.1829.
Van Soest, R.W.M., Lavaleye, M.S.S., 2005. Diversity and abundance of sponges in bathyal coral reefs of Rockall Bank, NE Atlantic, from boxcore samples. Mar. Biol. Res. 1, 338–349. https://doi.org/10.1080/17451000500380322.
van Weering, T.C.E., de Haas, H., de Stigter, H.C., Lykke-Andersen, H., Kouvaev, I., 2003. Structure and development of giant carbonate mounds at the SW and SE Rockall Trough margins, NE Atlantic Ocean. Mar. Geol. 198, 67–81. https://doi.org/10.1016/S0025-3227(03)00095-1.
Verity, P.G., Robertson, C.Y., Tronzo, C.R., Andrews, M.G., Nelson, J.R., Sieracki, M.E., 1992. Relationships between cell volume and the carbon and nitrogen content of marine photosynthetic nanoplankton. Limnol. Oceanogr. 37, 1434–1446. https://doi.org/10.4319/lo.1992.37.7.1434.
Vic, C., Naveira Garabato, A.C., Green, J.A.M., Waterhouse, A.F., Zhao, Z., Melet, A., et al., 2019. Deep-ocean mixing driven by small-scale internal tides. Nat. Commun. 10, 2099. https://doi.org/10.1038/s41467-019-10149-5.
Vlasenko, V., Stashchuk, N., 2018. Tidally induced overflow of the Faroese channels bottom water over the Wyville Thomson Ridge. J. Geophys. Res. Oceans 123, 6753–6765. https://doi.org/10.1029/2018JC014365.
Wagner, H., Purser, A., Thomsen, L., Jesus, C.C., Lundälv, T., 2011. Particulate organic matter fluxes and hydrodynamics at the Tisler cold-water coral reef. J. Mar. Syst. 85, 19–29. https://doi.org/10.1016/j.jmarsys.2010.11.003.
Weinbauer, M., Ogier, J., Maier, C., 2012. Microbial abundance in the coelenteron and mucus of the cold-water coral *Lophelia pertusa* and in bottom water of the reef environment. Aquat. Biol. 16, 209–216. https://doi.org/10.3354/ab00443.
White, M., Mohn, C., de Stigter, H., Mottram, G., 2005. Deep-water coral development as a function of hydrodynamics and surface productivity around the submarine banks of the Rockall Trough, NE Atlantic. In: Freiwald, A., Roberts, J.M. (Eds.), Cold-Water Corals and Ecosystems. Springer Berlin Heidelberg, Berlin, Heidelberg, pp. 503–514. https://doi.org/10.1007/3-540-27673-4_25.
White, M., Roberts, J.M., van Weering, T., 2007. Do bottom-intensified diurnal tidal currents shape the alignment of carbonate mounds in the NE Atlantic? Geo Mar. Lett. 27, 391–397. https://doi.org/10.1007/s00367-007-0060-8.
Wickham, H., 2007. Reshaping data with the reshape package. J. Stat. Software 21, 1–20.
Wickham, H., 2016. ggplot2: Elegant Graphics for Data Analysis. Springer-Verlag. New York Available at: https://ggplot2.tidyverse.org.
Wickham, H., Bryan, J., 2019. Readxl: read excel files. Available at: https://CRAN.R-project.org/package=readxl.
Wickham, H., Francois, R., Henry, L., Moller, K., 2021. dplyr: a grammar of data manipulation. Available at: https://CRAN.R-project.org/package=dplyr.
Wild, C., Mayr, C., Wehrmann, L., Schöttner, S., Naumann, M., Hoffmann, F., et al., 2008. Organic matter release by cold water corals and its implication for fauna–microbe interaction. Mar. Ecol. Prog. Ser. 372, 67–75. https://doi.org/10.3354/meps07724.
Wilke, C.O., 2019. Cowplot: streamlined plot Theme and plot Annotations for "ggplot2. Available at: https://CRAN.R-project.org/package=cowplot.
Witbaard, R., Duineveld, G.C.A., Van der Weele, J.A., Berghuis, E.M., Reyss, J.P., 2000. The benthic response to the seasonal deposition of phytopigments at the porcupine Abyssal Plain in the North East Atlantic. J. Sea Res. 43, 15–31. https://doi.org/10.1016/S1385-1101(99)00040-4.
Wolff, G.A., Boardman, D., Horsfall, I., Sutton, I., Davis, N., Chester, R., et al., 1995. The biogeochemistry of sediments from the Madeira Abyssal Plain - preliminary results. Int. Rev. Gesamten Hydrobiol. 80, 333–349.
Wright, S.W., Jeffrey, S.W., 1987. Fucoxanthin pigment markers of marine phytoplankton analysed by HPLC and HPTLC. Mar. Ecol. Prog. Ser. 38, 259–266.
Wright, S.W., Jeffrey, S.W., Mantoura, R.F.C., Llewellyn, C.A., Bjornland, T., Repeta, D., et al., 1991. Improved HPLC method for the analysis of chlorophylls and carotenoids from marine phytoplankton. Mar. Ecol. Prog. Ser. 77, 183–196.
Xie, Y., 2020. knitr: a general-purpose package for dynamic report generation in R. Available at: https://yihui.org/knitr/.
Yamamuro, M., Kayanne, H., 1995. Rapid direct determination of organic carbon and nitrogen in carbonate-bearing sediments with a Yanaco MT-5 CHN analyzer. Limnol. Oceanogr. 40, 1001–1005. https://doi.org/10.4319/lo.1995.40.5.1001.
Youngbluth, M.J., Bailey, T.G., Davoll, P.J., Jacoby, C.A., Blades-Eckelbarger, P.I., Griswold, C.A., 1989. Fecal pellet production and diel migratory behavior by the euphausiid *Meganyctiphanes norvegica* effect benthic-pelagic coupling. Deep-Sea Res. Part A Oceanogr. Res. Pap. 36, 1491–1501. https://doi.org/10.1016/0198-0149(89)90053-8.
Zapata, M., Rodríguez, F., Garrido, J.L., 2000. Separation of chlorophylls and carotenoids from marine phytoplankton: a new HPLC method using a reversed phase C8 column and pyridine-containing mobile phases. Mar. Ecol. Prog. Ser. 195, 29–45. https://doi.org/10.3354/meps195029.
Zaret, T.M., Suffern, J.S., 1976. Vertical migration in zooplankton as a predator avoidance mechanism. Limnol. Oceanogr. 21, 804–813. https://doi.org/10.4319/lo.1976.21.6.0804.
Zimmerman, A.R., Canuel, E.A., 2001. Bulk organic matter and lipid biomarker composition of chesapeake bay surficial sediments as indicators of environmental processes. Estuar. Coast Shelf Sci. 53, 319–341. https://doi.org/10.1006/ecss.2001.0815.